

## Biogeochemistry

October 2013, Volume 115, Issue 1-3, Pages 399-417

<http://dx.doi.org/10.1007/s10533-013-9843-3>

© Springer Science+Business Media Dordrecht 2013

Archimer  
<http://archimer.ifremer.fr>

The original publication is available at <http://www.springerlink.com>

# Strong gradient of benthic biogeochemical processes along a macrotidal temperate estuary: focus on P and Si cycles

Raimonet Melanie<sup>1, a, \*</sup>, Andrieux Loyer Françoise<sup>2</sup>, Ragueneau Olivier<sup>1</sup>, Michaud Emma<sup>1</sup>, Kerouel Roger<sup>2</sup>, Philippon Xavier<sup>2</sup>, Nonent Michel<sup>3</sup>, Memery Laurent<sup>1</sup>

<sup>1</sup> Laboratoire Des Sciences de l'Environnement Marin, UMR 6539, Institut Universitaire Européen de la Mer, Plouzané, France

<sup>2</sup> DYNECO Pelagos, IFREMER, Plouzané, France

<sup>3</sup> Service de Radiologie et Imagerie Médicale, CHU Brest et GETBO, Faculté de Médecine et des Sciences de la Santé, UBO, Brest, France

<sup>a</sup> Present address : UMR 7619 Sisyphe, Université Pierre et Marie Curie Paris VI, Paris, France

\*: Corresponding author : Mélanie Raimonet, email address : [melanie.raimonet@gmail.com](mailto:melanie.raimonet@gmail.com)

## Abstract:

This study aims to investigate the role of spatial and temporal physical, biological and biogeochemical gradients on sediment biogeochemistry along a macrotidal and Si-rich estuary. Scanning and biogeochemical analyses were performed in the inner, mid and outer Aulne Estuary (France) at four seasons. The inner estuary shows high diagenetic activity linked to fluid mud dynamics and river loads. The highest authigenic phosphorus (Aut-P) concentrations ever found in the literature are observed in the inner estuary ( $18 \mu\text{mol g}^{-1}$  PS sediment). This is explained by a combination of favorable factors, i.e. the high organic matter and nutrient loads, the reductive conditions, the freshwater properties (low pH,  $\text{OH}^-$ , sulfate and  $\text{Mg}^{2+}$  concentrations), the increase of particle residence time by the upward convergence of particles due to residual currents, and allochthonous riverine Aut-P. We suggest that the high  $\text{Si(OH)}_4$  concentrations ( $>400 \mu\text{M}$ ) may even increase Aut-P precipitation through the increase of Fe-P formation in these low salinity conditions. In the mid estuary, erosion-deposition dynamics dominate in point bars and lead to the succession of poor and rich organic and authigenic phosphorus layers, recording thus the seasonality of matter loads and its seasonal translocation from the inner estuary. In the outer estuary, deposition rates are high and constant and biogeochemical properties are characteristic of marine environments. The precipitation of Aut-P from free phosphate ( $\text{PO}_4^{3-}$ ) is lower than in the inner estuary and might be limited by higher  $\text{Mg}^{2+}$  concentrations in saline waters. This study highlights that small macrotidal estuaries, and especially their freshwater sediments, may constitute an important phosphorus sink through the precipitation of Aut-P. This precipitation could even be enhanced in fresh or brackish environments, thus increasing long term phosphorus storage and altering benthic fluxes of  $\text{PO}_4^{3-}$  to the pelagic ecosystem.

**Keywords:** Early diagenesis ; Silicate ; Phosphate ; Authigenic phosphorus ; Macrotidal ; Estuary

## 37 **1. Introduction**

38

39 Over the past century, estuarine and coastal ecosystems have suffered eutrophication in  
40 response to increased anthropogenic loads of nitrogen (N) and phosphorus (P) (Nixon 1995;  
41 Seitzinger et al. 2005). Eutrophication has led to drastic changes in N:P:Si ratios and ecosystem  
42 functioning (Cloern 2001; Ragueneau et al. 2002), resulting in seasonal limitations of  
43 phytoplankton growth by N, P and/or silicon (Si) (Conley 2000; Beucher et al. 2004). During the  
44 last decades, P and N have been identified to limit phytoplankton growth in fresh and marine  
45 waters, respectively (Smith 1984; Howarth and Marino 2006). Si and P limitations are now  
46 implicated in estuarine and coastal waters (Howarth et al. 2011) in response to Si retention - due  
47 to river damming (Conley et al. 1993) - and P removal - associated to the improvement in sewage  
48 treatment plants (Némery and Garnier 2006).

49 Nutrient loads and limitations not only depend on riverine fluxes, but also on benthic-  
50 pelagic coupling. In shallow ecosystems such as estuaries, benthic sediments constitute either 1) a  
51 nutrient source through the mineralization of deposited biogenic matter and diffusion processes  
52 generating benthic fluxes, and/or 2) a sink of deposited - allochthonous and/or autochthonous -  
53 biogenic matter (Prastka et al. 1998; Soetaert et al. 2000; Laruelle 2009). It is therefore very  
54 important to study the relative fate of N, P and Si upon the deposition of organic matter at the  
55 sediment-water interface, in particular in shallow ecosystems e.g. estuaries.

56 Along the land-sea continuum, estuaries are among the most productive ecosystems, but  
57 also the most hydrologically variable ones, due to river discharge, tides and winds (Day et al.  
58 1989; Cloern 2001; Aller 2004). As tides can lead to a succession of different sedimentary facies

59 in estuaries (Aller 1994), it is essential to determine the sedimentary properties that exert a  
60 profound influence on vertical distributions of chemical species. Estuaries are also characterized  
61 by sharp gradients of environmental conditions - pH, salinity, temperature, nutrient  
62 concentrations - which can lead to strong gradients of biogeochemical processes (Yamada and  
63 D'Elia 1980; Sharp et al. 1984), but also to interactions between biogeochemical cycles, e.g.  
64 between P and Si cycles (Tallberg et al. 2008).

65 Estuaries play a major role in the transport and transformation of key elements (e.g. P and  
66 Si) and their bioavailability in the coastal zone. Estuaries are characterized by high buffering  
67 capacity due to the quick adsorption and desorption of dissolved inorganic P (phosphate,  $\text{PO}_4^{3-}$ )  
68 onto and from particles (Froelich 1988; Sundby et al. 1992), which permit the transport of  
69 adsorbed  $\text{PO}_4^{3-}$  along the land-sea continuum and its progressive release in brackish and marine  
70 waters. The deposition and mineralization of organic P (Orga-P) also generates  $\text{PO}_4^{3-}$  in sediment  
71 pore waters. In oxic sediment,  $\text{PO}_4^{3-}$  quickly adsorbs onto mineral particles, and reacts with iron  
72 oxides to form iron-bound phosphorus (Fe-P), thus buffering benthic  $\text{PO}_4^{3-}$  fluxes to the water  
73 column (Sundby et al. 1992; Anschutz et al. 1998). In deep and anoxic sediments, Orga-P  
74 mineralization and Fe-P dissolution generate  $\text{PO}_4^{3-}$  which can precipitate - e.g., with  $\text{Ca}^{2+}$  - to  
75 form a less reactive authigenic phase (Aut-P) favoring P storage (Ruttenberg and Berner 1993;  
76 Slomp et al. 1996). However, Aut-P is not often measured and accounts for a small fraction of P  
77 in existing estuarine studies.

78 The Si cycle is generally less studied than N or P cycles in estuaries. The availability in  
79 dissolved Si (silicic acid,  $\text{Si}(\text{OH})_4$ ) is however essential for the growth of diatoms, which  
80 constitute 50-75 % of coastal phytoplankton production (Nelson et al. 1995). The incorporation

81 of Si by living organisms also participates in increasing the deposition rate of organic matter  
82 through the ballast effect of amorphous biogenic silica (Smetacek 1985). The amorphous silica -  
83 e.g., diatom skeleton, sponges, plants - settles at the sediment-water interface and dissolves into  
84  $\text{Si(OH)}_4$  that diffuses back to pelagic waters. As with  $\text{PO}_4^{3-}$ ,  $\text{Si(OH)}_4$  also undergoes sorption  
85 processes onto particles, in particular in resuspended sediments (Gehlen and Van Raaphorst  
86 2002).

87 Estuaries have however been given low attention with respect to Si-P interactions.  
88 Competition between Si and P cycles - i.e., between  $\text{Si(OH)}_4$  and  $\text{PO}_4^{3-}$  for sorption sites - were  
89 suggested in lakes, rivers and/or laboratory conditions (Hartikainen et al. 1996; Tuominen et al.  
90 1997; Mayer and Jarrell 2000; Koski-Vähälä et al. 2001).  $\text{Si(OH)}_4$  was shown to enhance  $\text{PO}_4^{3-}$   
91 desorption and benthic fluxes (Mayer and Jarrell 2000; Koski-Vähälä et al. 2001), prevent  $\text{PO}_4^{3-}$   
92 adsorption, but also increase iron-bound P (Fe-P) formation (Mayer and Jarrell 2000; Koski-  
93 Vähälä et al. 2001; Loucaides et al. 2010). Because high concentrations of  $\text{Si(OH)}_4$  could alter  
94 the P cycle, it is essential to investigate simultaneously benthic chemical species of Si and P  
95 cycles, and to consider and discuss the impact of Si-P interactions on the biogeochemistry of Si-  
96 enriched benthic sediments. Importantly, the role of  $\text{Si(OH)}_4$  has never been related to authigenic  
97 P (Aut-P) formation.

98 The Aulne Estuary - the main tributary flowing into the Bay of Brest (Fig. 1) - is a  
99 shallow macrotidal ecosystem characterized by high anthropogenic nutrient inputs (due to intense  
100 agricultural activities, fisheries and urbanization), Si inputs resulting from weathering of Si-  
101 enriched soils and terrestrial phytoliths, and intense hydrodynamic regime (e.g. high tidal range  
102 and currents). These properties of the Aulne Estuary may be favorable for Si-P interactions, as

103 recently suggested by the increased  $\text{PO}_4^{3-}$  benthic fluxes linked to high  $\text{Si}(\text{OH})_4$  concentrations of  
104 the Bay of Brest (Tallberg et al. 2008).

105 The aim of this study was to investigate the role of environmental factors on the benthic  
106 biogeochemical processes and the distribution of P and Si forms along an estuarine gradient.

107 This study was undertaken in benthic sediments of the Aulne Estuary, as a model of  $\text{Si}(\text{OH})_4$   
108 enriched sediments in a small macrotidal estuary.

109

## 110 **2. Methods**

111

### 112 2.1. Study site

113

114 Located in Northwestern France, the macrotidal Aulne Estuary (averaged tidal amplitude  
115 of 4 m, 35 km long; Fig. 1) receives N and Si enriched waters from the Aulne River that drains an  
116 area of about 1800 km<sup>2</sup> and brings annually 60 % of fresh water to the Bay of Brest. Nitrate  
117 ( $\text{NO}_3^-$ ) concentrations at the Aulne River outfall were maximal in winter ( $\sim 500 \mu\text{mol L}^{-1}$ ) and  
118 minimal in summer ( $\sim 100 \mu\text{M}$ ; Réseau ECOFLUX, <http://www-iuem.univ-brest.fr/ecoflux>;  
119 Table 1). Free  $\text{PO}_4^{3-}$  concentrations through the year were consistently low ( $\sim 1 \mu\text{M}$ ; Réseau  
120 ECOFLUX; Table 1) due to  $\text{PO}_4^{3-}$  adsorption onto particles (Mayer and Gloss 1980). Mean  
121  $\text{Si}(\text{OH})_4$  concentrations were close to  $130 \mu\text{M}$  with sporadic variations between 50 and  $200 \mu\text{M}$   
122 (Réseau ECOFLUX; Table 1). The oceanic climate of the region leads to higher precipitations -  
123 associated to frequent storms - in winter than in summer, thus modifying river discharge. In 2009,  
124 river flow ranged from  $1.7$  to  $189 \text{ m}^3 \text{ s}^{-1}$  (mean =  $24.4 \text{ m}^3 \text{ s}^{-1}$ ; Fig. 2). The spatial distribution of

125 salinity ranging from 0 to 35 throughout the Aulne Estuary depends on season, river discharge  
126 and tide. The concentrations of  $\text{NO}_3^-$ ,  $\text{PO}_4^{3-}$  and  $\text{Si}(\text{OH})_4$  decreased with salinity (Table 1) to 0-  
127 35, 0-0.5, and 0-10  $\mu\text{M}$ , respectively, in the Bay of Brest (Service d'Observation en Milieu  
128 Littoral SOMLIT, [somlit.epoc.u-bordeaux1.fr](http://somlit.epoc.u-bordeaux1.fr)).

129

## 130 2.2. Sampling design

131

132 Cruises were performed in February, May, July and October 2009. Three stations were  
133 located from upstream to downstream of the Aulne Estuary (A1, A2, A3; Fig. 1) at salinity of ~  
134 0, ~ 20 and ~ 30. Sampling was always performed at mid-tide (+/- 1.5 h) in subtidal shores. Note  
135 that the presence of highly consolidated and unpenetrable sediment at station A2 previously  
136 sampled in February and May prevented core sampling at the exactly same site in July and  
137 October. Core sampling was consequently performed 200 m downward the site previously  
138 sampled in February and May.

139 Gravity corer (UWITEC<sup>®</sup>) was used to sample plexiglass cores (9.5 cm diameter x 60 cm  
140 long). Corer weight was adjusted to allow 30 cm penetration into the sediment without disturbing  
141 the sediment-water interface.

142 Two sediment cores were sampled at each station in February, July and October - but not  
143 in May - to characterize the sedimentary structure by using Computer axial tomography (CAT  
144 scan). These cores were exposed to aerated waters in laboratory prior to their analysis. Three  
145 other cores were sampled at each station in February, May, July and October for assessment of

146 benthic biogeochemistry. These sediment cores were immediately sliced at a resolution of 0.5 cm  
147 (0-2 cm depth), 1 cm (2-4 cm depth), 2 cm (4-12 cm depth), and 4 cm (12-20 cm depth).  
148 Sediment sections were placed in sealed 50-ml centrifuge tubes containing Vectaspin 20 filters  
149 (0.45  $\mu\text{m}$  pore size, Whatman<sup>®</sup>) according to Andrieux-Loyer et al. (2008).

150 Interstitial waters were extracted by centrifuging the sub-sampled sediments at 3500 rpm  
151 for 10 min (2 times) at cooled temperature and later acidified to  $\text{pH} = 2$ . One aliquot of the  
152 extracted pore water was preserved at 4  $^{\circ}\text{C}$  for analyses of  $\text{Si}(\text{OH})_4^*$ ,  $\text{Fe}^{2+}$  and  $\text{Mn}^{2+}$   
153 concentrations and the other aliquot was frozen for  $\text{PO}_4^{3-\dagger}$ ,  $\text{NH}_4^+$  and  $(\text{NO}_3^- + \text{NO}_2^-)$  analyses  
154 (Andrieux-Loyer et al. 2008).

155 Comparisons were performed between our technique (pore waters extracted from  
156 sediments, centrifuged in a Vectaspin tube, and acidified) and Rhizons<sup>®</sup> (without any contact  
157 with air). The two extraction techniques showed similar results in  $\text{Fe}^{2+}$  concentrations,  
158 confirming that quick core slicing, centrifuging, acidification, and storage gave confident  
159 concentrations of dissolved species, and thus in particulate P forms.

160 The bulk sediment samples that were not centrifuged were stored at 4  $^{\circ}\text{C}$  for less than 15  
161 days to determine granulometry. Centrifuged sediments were freeze-dried during 48 h, put at 60  
162  $^{\circ}\text{C}$  to ensure the complete sediment dryness, and ground for further analyses of P forms in the  
163 solid fraction.

164

### 165 2.3. Laboratory analyses

---

\* Silicate (or orthosilicic acid) is noted  $\text{Si}(\text{OH})_4$  for simplification and is mainly present as  $\text{H}_4\text{SiO}_4$ .

† Inorganic phosphate (or orthophosphate) is noted  $\text{PO}_4^{3-}$  for simplification. The predominant forms are  $\text{HPO}_4^{2-}$  and  $\text{H}_2\text{PO}_4^-$  in fresh and marine waters.

166

167           The cores were analyzed with a Philips scanner (MX 8000 IDT 16) between 3 and 6 days  
168 after their sampling. Core tops were sealed with paraffin for stabilizing sediment according to  
169 Michaud et al. (2003) in the morning before the analysis. During the analysis, cores were  
170 horizontally placed on a table sliding through a crown consisting of a rotating X-ray source with  
171 x vertical receptors. The principle of this technique has been widely described in the literature  
172 (e.g., De Montety et al. 2003; Michaud et al. 2003). Core slices of 1 mm overlapping every 0.5  
173 mm were scanned with the power settings of 120 Kv, 45 mA and a pitch of 1. We used a matrix  
174 of  $512 \times 512$  and the field of view was 115, which gave a pixel resolution on each transverse  
175 section of 0.22 mm. The 2D longitudinal sections, which were perpendicularly reconstructed  
176 from the transverse sections, had a pixel resolution of 1 mm.

177           Sediment grain size analyses were performed using LS 200 Beckman Coulter laser  
178 granulometry. The fraction of fine particles - silt and clay ( $< 63 \mu\text{m}$ ) - was chosen to characterize  
179 sediment granulometry (Lesourd et al. 2003). Porosity was obtained after drying wet sediment of  
180 precise volume for 5 days, when the loss of weight was determined (Berner 1980).

181           P forms expressed in  $\mu\text{mol g}^{-1}$  were determined using the sequential analytical procedure  
182 detailed in Andrieux-Loyer et al. (2008) and adapted from widespread extraction methods  
183 (Psenner et al. 1988; Ruttenberg 1992; Aspila 1976). Adsorbed and iron-oxide bound P (Fe-P)  
184 was extracted in the first extraction step with dithionite-bicarbonate ( $0.1 \mu\text{M}$ , 8h,  $20^\circ\text{C}$ ). Na-  
185 acetate buffer ( $1 \mu\text{M}$ , pH=4, 6h,  $20^\circ\text{C}$ ) followed by  $\text{MgCl}_2$  wash ( $1 \mu\text{M}$ , pH=8, 0.5h,  $20^\circ\text{C}$ ) were  
186 then used to recover authigenic P (carbonate fluoroapatite  $\text{Ca}_5(\text{PO}_4, \text{CO}_3)_3\text{F}$ , biogenic  
187 hydroxyapatite  $\text{Ca}_{10}(\text{PO}_4)_6(\text{OH})_2$ ,  $\text{CaCO}_3$ -bound P) noted Aut-P (step 2). The detrital

188 fluoroapatite-bound P (Det-P) was determined in a third step of HCl (1  $\mu$ M) overnight. Organic P  
189 (Orga-P) was finally determined by ashing at 550 °C for 4h and using HCl (1  $\mu$ M) overnight  
190 (step 4).

191  $\text{PO}_4^{3-}$ ,  $\text{NH}_4^+$  and ( $\text{NO}_3^- + \text{NO}_2^-$ ) concentrations were analyzed using segmented flow  
192 analysis (SFA; Aminot et al., 2009) and  $\text{Si}(\text{OH})_4$  concentrations were determined with an  
193 AutoAnalyzer III (Bran+Luebbe<sup>®</sup>) using the method of Tréguer and Le Corre (1975).  $\text{Fe}^{2+}$   
194 concentrations were measured with the ferrozine method (Sarradin et al. 2005) and  $\text{Mn}^{2+}$  with the  
195 leuco-malachite green method (Resing and Mottl 1992), both adapted for SFA. The precision of  
196 the analyses was 0.5 %.

197

#### 198 2.4. Data processings

199

200 Pictures of longitudinal sections were obtained in dicom format to be later analyzed by  
201 image J<sup>®</sup> software. We analyzed the sedimentary structure of each core by using a tomogram  
202 representing tomographic intensities (TI) expressed in Hounsfield units (HU) along a longitudinal  
203 plane for the entire length of the core (Gagnoud et al. 2009; Michaud et al. 2003). The calibration  
204 gave specific values for tomographic intensities according to analyzed materials (i.e.,  $\text{TI}_{\text{air}} = -$   
205  $1000$ ;  $\text{TI}_{\text{water}} = 0$ ;  $\text{TI}_{\text{calcite}} = 2500$ ). To simplify illustrations, picture and TI profile are presented for  
206 only one core because of the low variability of duplicates. Duplicate variability was studied in  
207 February and July at stations A2 and A3. At each sediment depth, the variability was very low in

208 the outer estuary ( $CV^\ddagger < 10\%$ ) and slightly higher in the mid estuary ( $CV < 20\%$ ). Higher  
209 heterogeneity between duplicates was only locally observed below 5 cm depth, with CV reaching  
210 a maximum of 50 % at A3 and 60-80 % at A2 at some local depths. This local heterogeneity in  
211 deep sediment layers was mostly explained by the presence of a rock or bioturbation in the outer  
212 estuary, and by a small vertical shift of deep layers between duplicates in the mid estuary because  
213 of the sloping core layers. Except these local and deep heterogeneities, the general form of TI  
214 profiles was similar between duplicates. This confirms that the analysis of one core is enough to  
215 highlight the sedimentary facies at each station.

216 Surfer<sup>®</sup> software was used to interpolate measured values year round and create contour  
217 maps for P form concentrations, dissolved species concentrations, and dissolved species molar  
218 ratios (i.e.,  $NH_4^+ : PO_4^{3-}$  and  $Fe^{2+} : PO_4^{3-}$  ratios).

219 All statistical analyses were performed with R software (<http://cran.r-project.org>). The  
220 normality and homoscedasticity of data sets were first assessed with Shapiro and Bartlett tests to  
221 determine the suitability of these data sets for parametric or non-parametric statistical tests.  
222 Wilcoxon or *t*-tests were performed to determine significant differences of porosity and grain size  
223 between stations or seasons. Pearson or Spearman correlations were used to evaluate  
224 relationships between all measured variables (Orga-P, Fe-P, Aut-P, Det-P,  $PO_4^{3-}$ ,  $NH_4^+$ , ( $NO_3^- +$   
225  $NO_2^-$ ),  $Si(OH)_4$ ,  $Fe^{2+}$ ,  $Mn^{2+}$ , porosity). For all tests, values were considered significant at  $p <$   
226 0.05.

227

---

<sup>‡</sup> CV is the coefficient of variation e.g. the standard deviation as a percentage of the mean

## 228 **3. Results**

229

### 230 3.1. Surface sediment grain size

231

232 Even not significant (Table 2), the proportion of fine sediments ( $\% < 63 \mu\text{m}$ ) in surface  
233 sediments was slightly lower in February ( $78 \pm 6 \%$ ) than during other seasons ( $82 \pm 3 \%$ ; Table  
234 1) in the inner estuary (station A1). The proportion of fine surface sediments was lower in the  
235 intermediate estuary (station A2; 37-64 %) than at stations A1 and A3 ( $> 70 \%$ ; Table 1).

236

### 237 3.2. Porosity and salinity

238

239 In the inner estuary (station A1), porosity in surface sediments was significantly lower in  
240 February (0.82; Fig. 3, A1) compared to other months ( $> 0.9$ ; Table 2). The porosity decreased  
241 with depth from 0.82 to 0.75 in February and from 0.95 to 0.8 in May, July and October. The  
242 intermediate estuary (station A2) showed a particular pattern with layers of low (0.65-0.75) and  
243 high porosity (0.8-0.9) alternated along the core in February, July and October (Fig. 3, A2), but  
244 profiles decreasing progressively over depth in May (0.88 to 0.6). In the outer estuary (station  
245 A3), the porosity decreased with depth from 0.88 to 0.76 except some local discontinuities in July  
246 and October (Fig. 3, A3). Contrary to the vertical decrease in porosity, pore water salinity was  
247 constant over depth in May or very slightly increased along each core in February (analyses not

248 performed in July and October), and increased from station A1 to station A3 (Khalil et al.  
249 submitted).

250

### 251 3.3. Tomographic intensity

252

253 In the inner estuary, the tomogram indicated two different levels of TI in February and  
254 July (Fig. 3, A1). A layer of low density sediments ( $TI < 400$  HU), corresponding to fluid muds  
255 observed during core samplings, was pointed out at 0-3 cm depth in February and at 0-15 cm  
256 depth in July, while more dense sediments ( $TI = 700$  HU) were observed deeper. Homogeneous  
257 TI values (350-450 HU) were measured over depth in October, when fluid muds were observed  
258 throughout whole cores.

259 In the mid estuary, TI values varied over a large range over depth (200 to  $> 1100$  HU; Fig.  
260 3, A2). In February, the lowest density ( $< 400$  HU) was measured at 0-2 cm, while the highest  
261 and very variable density (600 to 1100 HU) was observed at 3-20 cm. Two thick bands of white  
262 color on the CAT scan pictures indicated particularly dense deposits (1100 HU) at 12 and 14 cm  
263 depth. These dense deposits ( $> 1100$  HU) were found at 6 and 8 cm depth in July. They were  
264 separated by relatively soft deposits ( $TI \sim 200$  HU; plant detritus observed during core slicing).  
265 More (800 HU) and less (200-500 HU) dense deposits alternated every 1 or 2 cm at 0-15 cm.  
266 Below 15 cm depth, the TI range was smaller (500 to 800 HU). In October, we observed the same  
267 pattern as in July. The same dense deposits (TI value  $> 1000$  HU) were observed at 0-2, 6 and 8  
268 cm depth. These dense layers were still separated by very soft sediments (200 HU) at 4, 7, and 9

269 cm depth.

270 In the outer estuary, deposit properties were less variable over depth (500-800 HU) than in  
271 the mid estuary, but varied over the seasons (Fig. 3, A3). In February, the density of deposits  
272 averaged at 500 HU, whereas four layers of denser deposits (800 HU) appeared at 10, 12, 16 and  
273 20 cm depth. In July, the same dense deposits (800 HU) were observed 2-3 cm deeper and a new  
274 layer of dense sediments appeared at 10 cm depth. In October, the same dense deposits occurred  
275 3-4 cm deeper than in July (at 16, 18, 22 and 26 cm depth) and a new layer of dense sediments  
276 appeared at 10 cm depth (800 HU).

277

#### 278 3.4. Particulate P forms

279

280 In the inner estuary (station A1), maximal Orga-P concentrations occurred in surface  
281 sediment in July (up to  $15.6 \mu\text{mol g}^{-1}$ ; Fig. 4, A1). Orga-P concentrations generally decreased  
282 with depth, with the lowest concentrations occurring in February and October ( $< 6 \mu\text{mol g}^{-1}$ ). Fe-  
283 P profiles showed a relatively similar pattern as those of Orga-P. The lowest concentrations  
284 occurred in depth in February and October (about  $13\text{-}15 \mu\text{mol g}^{-1}$ ) and coincided with Aut-P  
285 maximal concentrations ( $16\text{-}18 \mu\text{mol g}^{-1}$ ). Low concentrations and seasonal variations of Det-P  
286 were observed ( $5.4 \pm 1.1 \mu\text{mol g}^{-1}$ ).

287 The mid estuary (station A2) was characterized by a vertical succession of Orga-P poor  
288 and rich layers with two marked gaps ( $< 1 \mu\text{mol g}^{-1}$ ) in May (6-12 cm) and October (8-20 cm;  
289 Fig. 4, A2). As observed in the inner estuary, these low Orga-P concentrations in February and

290 May were observed with the lowest Fe-P concentrations ( $< 8 \mu\text{mol g}^{-1}$ ) and the highest Aut-P  
291 concentrations. In October, low Orga-P concentrations coincided however with the highest Fe-P  
292 and Aut-P concentrations. Det-P concentrations generally increased with depth and from  
293 February to October.

294 The outer estuary (station A3) showed relatively little seasonal variations regarding the  
295 vertical profiles of phosphorus forms. Orga-P and Fe-P concentrations decreased with depth (Fig.  
296 4, A3), whereas Aut-P and Det-P concentrations varied little over depth (annual and vertical  
297 average concentrations of Aut-P =  $6.9 \pm 1.6 \mu\text{mol g}^{-1}$  and Det-P =  $5.4 \pm 1.1 \mu\text{mol g}^{-1}$ ).

298

### 299 3.5. Dissolved chemical species

300

301 At all stations, the oxygen penetration depth varied from 0.5 mm to 5 mm (Khalil et al.  
302 submitted). The limit between suboxic ( $0.2\text{-}0.0 \text{ mg L}^{-1}$ ) and anoxic ( $0.0 \text{ mg L}^{-1}$ ) conditions -  
303 according to the classification of Tyson and Pearson (1991) - was thus always reached within the  
304 first 5 mm. All pore water  $\text{NO}_3^-$  profiles showed a strong decrease of concentrations with depth  
305 (Fig. 5). At all stations,  $\text{NO}_3^-$  was below the detection limit at a depth of 2-4 cm. The lowest  
306 penetration depths were observed in May (A1) or in July (A2, A3).

307 In the inner estuary, pore water  $\text{PO}_4^{3-}$  concentrations were always low ( $< 12.1 \mu\text{M}$ ; Fig. 5,  
308 A1). Pore water concentrations of  $\text{NH}_4^+$ ,  $\text{Mn}^{2+}$ ,  $\text{Fe}^{2+}$  and  $\text{Si}(\text{OH})_4$  increased with depth at all  
309 seasons and were much higher in February and May (up to 2800, 35, 900 and 580  $\mu\text{M}$ ,  
310 respectively).  $\text{NH}_4^+:\text{PO}_4^{3-}$  and  $\text{Fe}^{2+}:\text{PO}_4^{3-}$  ratios increased up to 300, especially in February and

311 May (Fig. 6, A1).

312 In the mid estuary, on the opposite to the inner estuary,  $\text{PO}_4^{3-}$  concentrations sharply  
313 increased with depth, especially in February and July (up to 259 and 193  $\mu\text{M}$ ; Fig. 5, A2).  $\text{NH}_4^+$   
314 concentrations never exceeded 1000  $\mu\text{M}$  and decreased from February to October.  $\text{Mn}^{2+}$ ,  $\text{Fe}^{2+}$  and  
315  $\text{Si}(\text{OH})_4$  were characterized by very high concentrations in subsurface sediment in February and  
316 May (550-800, 1500-3000 and 28-60  $\mu\text{M}$ , respectively).  $\text{NH}_4^+:\text{PO}_4^{3-}$  ratios were higher than 16 in  
317 surface layers in February and in deepest layers in May but never reached the high values  
318 observed at A1 (Fig. 6, A2). The highest  $\text{Fe}^{2+}:\text{PO}_4^{3-}$  ratios occurred in May but never exceeded  
319 70.

320 In the outer estuary, dissolved species showed vertical distributions observed typically for  
321 sediments undergoing diagenesis.  $\text{PO}_4^{3-}$ ,  $\text{NH}_4^+$  and  $\text{Si}(\text{OH})_4$  concentrations increased with depth,  
322 while  $\text{Mn}^{2+}$  and  $\text{Fe}^{2+}$  showed maximal subsurface concentrations (Fig. 5, A3). The deepest part  
323 of the sediment core contained the highest  $\text{PO}_4^{3-}$  concentrations in May, and the highest  $\text{NH}_4^+$  and  
324  $\text{Si}(\text{OH})_4$  concentrations in July.  $\text{Mn}^{2+}$  and  $\text{Fe}^{2+}$  showed maximal subsurface concentrations never  
325 exceeding 252  $\mu\text{M}$  and 42  $\mu\text{M}$ , respectively, in October. On the opposite to the inner estuary,  
326  $\text{NH}_4^+:\text{PO}_4^{3-}$  and  $\text{Fe}^{2+}:\text{PO}_4^{3-}$  ratios rarely exceeded values of 16 and 2, respectively, and decreased  
327 over depth (Fig. 6, A3).

328

329 3.6. Correlations between benthic properties

330

331 Pearson correlations were calculated on the matrix of measured variables (Table 3). In the

332 inner and outer estuary (stations A1 and A3), Orga-P was positively correlated to ( $\text{NO}_3^- + \text{NO}_2^-$ ),  
333 Fe-P and porosity, and negatively correlated to  $\text{Si}(\text{OH})_4$ ,  $\text{NH}_4^+$ ,  $\text{Mn}^{2+}$  and Det-P. In the mid and  
334 outer estuary (stations A2 and A3), positive correlations were observed for  $\text{Si}(\text{OH})_4$  vs  $\text{PO}_4^{3-}$ ,  
335  $\text{Si}(\text{OH})_4$  vs  $\text{NH}_4^+$ , and  $\text{PO}_4^{3-}$  vs  $\text{NH}_4^+$ . Negative correlations of Orga-P with  $\text{PO}_4^{3-}$  and Aut-P were  
336 only found in the inner estuary. At this station (A1), positive correlations were observed between  
337  $\text{Si}(\text{OH})_4$ ,  $\text{NH}_4^+$ ,  $\text{Fe}^{2+}$ ,  $\text{Mn}^{2+}$  and Det-P vs Aut-P, while negative correlations were observed for  
338  $\text{PO}_4^{3-}$ , Fe-P and Orga-P vs Aut-P, and  $\text{NH}_4^+$  and  $\text{Si}(\text{OH})_4$  vs  $\text{PO}_4^{3-}$ . In the mid estuary, Aut-P was  
339 positively correlated with Fe-P, and negatively correlated with Aut-P.

340

#### 341 **4. Discussion**

342

##### 343 **Enhancement of benthic biogeochemical processes in inner estuary**

344

345 The inner estuary is characterized by the presence of fluid muds (Fig. 3, A1). This  
346 estuarine feature is commonly observed at water salinity ranging between 0 and 10 due to  
347 suspended matter flocculation, sedimentation, upward transport by residual bottom currents, and  
348 tidal asymmetry (Allen et al. 1980; Postma 1967; Woodruff et al. 2001). The increase of fluid  
349 mud thickness over the year - from ~ 2 cm in February to 15 cm in July and > 20 cm in October  
350 (Fig. 3) - is associated to the river discharge decrease (Fig. 2) and the progressive accumulation  
351 of sediments in the inner Aulne Estuary (Bassoulet 1979). The seasonal increase of the fluid mud  
352 thickness leads to seasonal variations of vertical profiles of porosity and particulate and dissolved

353 species (Figs. 3, 4 and 5) which are correlated (Table 3), especially Fe-P and Orga-P. The high  
354 Fe-P concentrations in fluid muds highlight the potential stocks of quickly available P due to the  
355 sorption of P onto sediments (Mayer and Gloss 1980). The high Orga-P concentrations show that  
356 fluid muds are also enriched in organic matter. These results are consistent with the general  
357 description of fluid muds that are considered as reactors for intense organic matter recycling  
358 (Aller 2004).

359         The high pore water  $\text{NH}_4^+$ ,  $\text{Mn}^{2+}$ ,  $\text{Fe}^{2+}$  and  $\text{Si(OH)}_4$  concentrations in the inner estuary in  
360 February indicate (1) the high benthic mineralization resulting from the high loads of organic and  
361 silicified matter associated to fluid muds, (2) the sediment re-oxidation after erosion, and (3) the  
362 presence of older sediments. High pore water concentrations of  $\text{NH}_4^+$ ,  $\text{Mn}^{2+}$  and  $\text{Fe}^{2+}$  (Fig. 5, A1)  
363 and low oxygen penetration depth (< 5 mm; Khalil et al. submitted) in the inner estuary in winter,  
364 when fluid muds are absent, highlight intense organic matter degradation mediated by bacteria  
365 (Berner 1980; Soetaert et al. 1998), thus leading to the vertical decrease of Orga-P concentrations  
366 (Fig. 4, A1). Even if fluid muds are absent in winter (during the short period of higher river  
367 discharge), organic matter is brought year-round by the accumulation of fluid muds in the inner  
368 estuary, which increase benthic mineralization processes. High pore water  $\text{Si(OH)}_4$   
369 concentrations in the inner estuary indicate that amorphous Si is associated with this organic  
370 matter and characterized by intense benthic dissolution (Berner 1980). This load of amorphous Si  
371 was confirmed by the high amorphous Si concentrations observed in the Aulne surface freshwater  
372 in February (Raimonet et al. 2013). Additionally, the high discharge of river waters enriched with  
373  $\text{O}_2$  and  $\text{NO}_3^-$  lead to an increase of  $(\text{NO}_3^- + \text{NO}_2^-)$  concentration and penetration in surface  
374 sediments. The enhanced penetration depth of highly oxidative  $\text{O}_2$  and  $\text{NO}_3^-$  in February then

375 intensifies mineralization processes (Berner 1980), anaerobic reduced metabolite re-oxidation  
376 (Aller et al. 2004) and decreases the use of other electron acceptors. Increasing  $Mn^{2+}$  and  $Fe^{2+}$   
377 concentrations and decreasing Fe-P concentrations over depth suggest that Mn and Fe oxides  
378 facilitate mineralization down to  $(NO_3^- + NO_2^-)$  penetration depth in sediment. These high  
379 concentrations of  $NH_4^+$ ,  $Mn^{2+}$ ,  $Fe^{2+}$  and  $Si(OH)_4$  (Fig. 5, A1) and the vertical decrease in Orga-P  
380 and Fe-P concentrations which are particularly high in surface layers (Fig. 4, A1) highlight thus  
381 the high mineralization activity of re-oxidized sediments after fluid mud displacement, which has  
382 already been observed in the Amazon Shelf (Aller 2004). Finally, the erosion of fluid muds  
383 exposes older and more compact sediments, which were similar by low %  $< 63 \mu m$  (and porosity,  
384 this study) to sediments collected in the Seine and Palmones estuaries after flooding events  
385 (Lesourd et al. 2003; Avilés and Niell 2005). The presence of reducing conditions in the old  
386 exposed sediments in the inner estuary, in association with higher initial P-bearing components  
387 (Orga-P and Fe-P) and lower salinity compared to the mid and outer estuary, might have  
388 enhanced the precipitation of Aut-P (detailed below), as all these conditions are favorable for  
389 Aut-P precipitation (Ruttenberg and Berner 1993; Slomp et al. 1996).

390         The precipitation of Aut-P in sediment is highlighted by  $NH_4^+ : PO_4^{3-}$  and  $Fe^{2+} : PO_4^{3-}$   
391 ratios much higher than 16 and 2, respectively (Fig. 6). High  $NH_4^+ : PO_4^{3-}$  ratios indicate that  
392 mineralization alone cannot explain the vertical profiles of dissolved species, and that  $NH_4^+$   
393 formation and/or  $PO_4^{3-}$  removal may take place in these sediments (Ruttenberg and Berner 1993).  
394 Even if  $NH_4^+$  might have formed from dissimilatory  $NO_3^-$  reduction to  $NH_4^+$  (DNRA) (Laverman  
395 et al. 2006; Gardner and McCarthy 2009), the production of  $NH_4^+$  would have not led to such  
396 high  $NH_4^+ : PO_4^{3-}$  ratios in the inner estuary in February. Moreover,  $Fe^{2+} : PO_4^{3-}$  ratios would have

397 been close to the theoretical ratio of 2 iron oxyhydroxide molecules linked to each  $\text{H}_2\text{PO}_4^-$  ion  
398 (Lijklema 1977; Lehtoranta and Heiskanen 2003). In our study, the high  $\text{Fe}^{2+}:\text{PO}_4^{3-}$  ratios (Fig.  
399 6) indicate  $\text{Fe}^{2+}$  release during Fe oxide reduction, and  $\text{PO}_4^{3-}$  removal through precipitation.  
400 These simultaneously high  $\text{NH}_4^+:\text{PO}_4^{3-}$  and  $\text{Fe}^{2+}:\text{PO}_4^{3-}$  ratios - previously reported for freshwater  
401 sediments (Hartzell et al. 2010) -, and the low  $\text{PO}_4^{3-}$  concentrations ( $< 5 \mu\text{M}$ ) are consistent with  
402 the presence of Aut-P (Slomp et al. 1996), confirming that Aut-P precipitation happened (Berner  
403 1980).

404         Precipitation of Aut-P generally results from the removal of free  $\text{PO}_4^{3-}$  in pore waters,  
405 issued from Fe-P dissolution and from Orga-P mineralization in anoxic conditions (Ruttenberg  
406 and Berner 1993; Reimers et al. 1996; Slomp et al. 1996). In this study, the negative correlations  
407 of Fe-P and Orga-P vs Aut-P (Table 3), and the vertical decrease of Fe-P concentrations (Fig. 7)  
408 in the inner estuary indicate that Aut-P precipitates from  $\text{PO}_4^{3-}$  originated from both Orga-P and  
409 Fe-P. Such high Aut-P concentrations ( $> 14 \mu\text{mol g}^{-1}$ ) have never been observed in other systems  
410 (Table 4). The intense precipitation of Aut-P in the inner estuary results of the presence of  
411 reducing conditions in older sediments, which conditions are known to increase the preservation  
412 of P (Jilbert et al. 2011) and thus Aut-P precipitation (Slomp et al. 1996). The presence of lower  
413 pH, sulfate and  $\text{Mg}^{2+}$  concentrations in fresh compared to marine waters also favors the formation  
414 of Aut-P by limiting the competition of  $\text{PO}_4^{3-}$  with  $\text{OH}^-$  and sulfate for sorption sites, and the  
415 competition of  $\text{Mg}^{2+}$  with  $\text{Ca}^{2+}$  (Caraco et al. 1989; Mayer and Jarrell 2000; Gunnars et al. 2004;  
416 Hyacinthe and Van Cappellen 2004). Other factors - that have been shown to potentially  
417 constrain sorption processes along estuaries, in laboratory conditions - are also expected to  
418 influence the precipitation of Aut-P, e.g. specific surface area and mineral composition of

419 particles, cation exchange capacity, bacterial uptake, presence of arsenate, organic, humic or  
420 fulvic acids (Fontes and Weed 1996; Sundareshwar and Morris 1999; Violante et al. 2002; Cao et  
421 al. 2007; Loucaides et al. 2010). More studies are however needed to investigate the role of these  
422 factors in estuarine environments.

423         As the formation of Fe-P was reported to be highly increased in the presence of  $\text{Si(OH)}_4$   
424 that leads to Si-enriched Fe oxides, especially at low pH (Mayer and Jarrell 2000), we also  
425 explored the indirect role of high  $\text{Si(OH)}_4$  concentrations in the precipitation of Aut-P in inner  
426 estuary where the freshwater is more Si-enriched and acid than marine waters. In this study,  
427  $\text{Si(OH)}_4$  concentrations associated with high Aut-P concentrations reach more than 400  $\mu\text{M}$  in the  
428 inner estuary in February. We hypothesize that high  $\text{Si(OH)}_4$  concentrations increase first Fe-P  
429 formation during Fe oxidation in surface sediments, which is known to favor Aut-P formation  
430 (Slomp et al. 1996). In the deepest anoxic sediments, high  $\text{Si(OH)}_4$  concentrations saturate  
431 mineral sorption sites, and thus release free  $\text{PO}_4^{3-}$  (Mayer and Jarrell 2000). High free  $\text{PO}_4^{3-}$   
432 concentrations mediated by high  $\text{Si(OH)}_4$  concentrations favor then Aut-P formation observed in  
433 these same layers. The high  $\text{Si(OH)}_4$  concentrations suggest that continuous and high dissolution  
434 of Si-enriched Fe oxides happen in deep sediments. Even if high  $\text{Si(OH)}_4$  concentrations and  
435 resuspension events were shown to potentially enhance benthic fluxes of  $\text{PO}_4^{3-}$  (Tallberg et al.  
436 2008; de Vicente et al. 2010), the present study also suggests that these conditions could  
437 indirectly increase Aut-P precipitation in low salinity waters.

438         Additionally to these numerous favorable conditions for Aut-P precipitation in inner  
439 estuarine sediments, Aut-P might have also been partly brought by upper riverine freshwaters.  
440 Aut-P concentrations in surface sediments reached up to 11  $\mu\text{mol g}^{-1}$  which can attest of erosion

441 of surface Aut-P poor sediments and/or of loads of allochthonous riverine Aut-P. Aut-P indeed  
442 preferentially precipitates in freshwater environmental conditions i.e. low pH, sulfate and  $Mg^{2+}$   
443 concentrations (see above). The decrease of surface Aut-P concentrations towards the outer  
444 estuary indicates the dilution and the settlement of Aut-P along the estuary. The higher Aut-P  
445 contents in the inner estuary thus results from a combination of reducing conditions, high loads of  
446 Orga-P, Fe-P and Aut-P, and the presence of freshwaters (low pH,  $OH^-$ , sulfate and  $Mg^{2+}$   
447 concentrations, high  $Si(OH)_4$  concentrations).

448         Regardless of the factors leading to Aut-P precipitation, the formation of Aut-P both (1)  
449 decreases  $PO_4^{3-}$  fluxes, and (2) increases P retention. The trapping of  $PO_4^{3-}$  through Aut-P  
450 precipitation might indeed decrease benthic fluxes of  $PO_4^{3-}$  to the water column, which means  
451 that benthic fluxes may have even been higher if  $PO_4^{3-}$  reprecipitation into Aut-P had not  
452 occurred. Aut-P forms - which have a higher potential of long term sinking in comparison with  
453 the more reactive P forms - also contribute to an efficient storage of P in benthic sediments  
454 (Ruttenberg and Berner 1993). The contribution of Aut-P formation in P storage in the inner  
455 Aulne Estuary ranges between 24 and 36 % of total P forms regardless of the season (not shown),  
456 agreeing with the high values (28 to 50 %) reported previously (Ruttenberg and Berner 1993;  
457 Andrieux and Aminot 1997), and suggesting high potential for long term P storage in the inner  
458 estuarine sediments.

459

460         **Role of point bar hydrodynamics in modulating the benthic biogeochemistry in the**  
461 **mid-estuary**

462

463           The succession of sediment layers highlights the turbulent hydrodynamic conditions (e.g.  
464 bottom currents, tides) in mid estuarine point bars. Turbulent hydrodynamic conditions in  
465 estuaries are generally associated to low concentrations of clay, organic matter and chlorophyll a  
466 (Moreno and Niell 2004). In our study, the low clay and silt contents and the generally lower  
467 Orga-P than Det-P concentrations in the mid estuary confirm highly dynamic conditions. The  
468 vertically heterogeneous sediment tomographic intensity observed in CAT scan cores (Fig. 3, A2)  
469 and the succession of muddy and detrital sediments (described above) moreover indicate the  
470 variability of dynamic conditions over time in the mid estuary, where the highest tidal energy  
471 occurs (Dyer 1989). Related to intense erosion-deposition events, the vertical heterogeneity in  
472 sediment cores was also observed along and across the mid estuary through an extensive  
473 investigation of spatial heterogeneity of pore water  $\text{Si}(\text{OH})_4$  profiles (Raimonet et al. 2013). High  
474 heterogeneity in sediments from the mid Aulne Estuary is expected and consistent with the  
475 highest variability observed in the mid Palmones and Penzé estuaries (Avilés and Niell 2005;  
476 Andrieux-Loyer et al. 2008) resulting from the hydrodynamic regime (Dyer 1989).

477           Contrary to the inner estuary, Aut-P concentrations do not increase with depth in the mid  
478 estuary but are associated to a succession of poor and enriched layers (Fig. 4), consistent with the  
479 presence of less and highly dense sediments (Fig. 3). The succession of layers of different  
480 properties suggests that the properties of sediment loads vary over time, each layer corresponding  
481 to different periods and origins. The Aut-P enriched layers suggest the translocation and  
482 deposition of freshwater or less marine sediments, as Aut-P preferentially precipitates in  
483 freshwater environmental conditions (as detailed above). The Aut-P present in subsurface  
484 sediment layers might have been formed upstream, e.g. in the river or the inner estuary, and then

485 transported to the mid estuary. The presence of high  $\text{Mn}^{2+}$ ,  $\text{Fe}^{2+}$  and  $\text{Si(OH)}_4$  concentrations in  
486 these same Aut-P enriched layers confirms that this translocation from the inner to the mid  
487 estuary might happen.

488         The high  $\text{Mn}^{2+}$  and  $\text{Fe}^{2+}$  concentrations, associated to high  $\text{Si(OH)}_4$  concentrations in  
489 subsurface layers in February and May in the mid-estuary (Fig. 5, A2), also highlight the  
490 presence of detrital terrestrial materials in deposits. The co-occurrence of these high  
491 concentrations might indeed result from the dissolution of the generally high Fe and Mn oxide  
492 concentrations associated with detrital terrestrial materials (Aller et al. 2004). These layers might  
493 result from the deposition of the terrestrial plant material exported from river and estuarine  
494 borders to estuarine waters (Bassoulet 1979), which commonly happen in temperate macrotidal  
495 estuaries during winter (Anderson et al. 1981). The export of silicified plants growing in  
496 estuarine marshes - mainly *Phragmites australis* in the Aulne Estuary - is known to be high after  
497 the high productive period in fall and during the high winter river discharge (Findlay et al. 1990;  
498 Querné 2011). This is consistent with the export of Si enriched materials and the high amorphous  
499 Si concentrations observed in February in the upper estuary (80  $\mu\text{M}$ ; Raimonet et al. 2013). A  
500 part of this exported matter may settle in mid estuarine point bars. It is however difficult to go  
501 further on the correspondence between layers and matter origin, because of the erosion-  
502 deposition cycles that perturb the vertical sequence.

503         The vertical profiles of particulate and dissolved matter and the scan images allow,  
504 however, estimating net seasonal deposition and erosion rates. The temporal deepening of the  
505 maximal subsurface  $\text{Mn}^{2+}$ ,  $\text{Fe}^{2+}$  and  $\text{Si(OH)}_4$  concentrations (observed at 1-4 cm in February, and  
506 at 2-7 cm in May; Fig. 5, A2) suggests the deposition of ~ 1-3 cm of sediment between February

507 and May. TI and CAT scan cores also show that sediment erosion happens between May and July  
508 (Fig. 3, A2). After erosion, older sediments - that were initially deeper - are exposed to pelagic  
509 waters. In contrast to the inner estuary (A1) where the downward displacement of fluid muds in  
510 February leads to high  $\text{NH}_4^+$ ,  $\text{Mn}^{2+}$ ,  $\text{Fe}^{2+}$  and  $\text{Si}(\text{OH})_4$  concentrations, sediments in the mid  
511 estuary have lower concentrations after erosion. These lower concentrations in mid compared to  
512 inner estuarine sediments after erosion are related to the presence of coarser sediments associated  
513 to lower porosity and lower organic matter content (e.g. Orga-P concentrations; Fig. 4, A2) due to  
514 more turbulent hydrodynamic conditions.

515         Such as in the inner estuary, evidence of *in situ* Aut-P precipitation in the mid Aulne  
516 Estuary is indicated by  $\text{NH}_4^+ : \text{PO}_4^{3-}$  and  $\text{Fe}^{2+} : \text{PO}_4^{3-}$  ratios higher than 16 and 2, respectively (Fig.  
517 6, A2), and by the negative correlation between Aut-P and Orga-P (Table 3). Vertically stable Fe-  
518 P concentrations in the mid estuary in October indicate that  $\text{PO}_4^{3-}$  leading to high Aut-P  
519 concentrations is not originated from Fe-P dissolution, but rather from Orga-P oxidation in the  
520 mid estuary (mirror profiles of Orga-P and Aut-P; Fig. 7). The decrease of  $\text{NH}_4^+ : \text{PO}_4^{3-}$  down to  
521 12 cm emphasizes that the remineralization of P relative to N increases with depth, consistent  
522 with the increasingly reductive conditions (Jilbert et al. 2011). As the effect of high  $\text{Si}(\text{OH})_4$   
523 concentrations on the benthic P cycle is mainly mediated through the increased formation of Fe-  
524 P, the preferential origins of Aut-P from Orga-P indicate that the interactions between Si and P  
525 cycles may be low in the mid estuary.

526

527         **Marine-type benthic biogeochemistry in the outer estuary**

528

529 Continuous deposition of sediments takes place throughout the year in the outer estuary.  
530 The net deposition rate is high (2-3 cm) from February to July and even higher (~ 4 cm) from  
531 July to October (Fig. 3). Lower hydrodynamic energy - explaining high deposition rates - leads to  
532 classical diagenetic profiles and low seasonal variability for solid and dissolved species in the  
533 outer estuary. During the productive period in May, chlorophyll a concentrations were higher  
534 (Raimonet 2011), and expectedly related to the occurrence of the maximal Orga-P concentrations  
535 in surface sediments, and the vertical decrease of Orga-P and Fe-P concentrations. In contrast to  
536 the inner and mid estuary, the lowest Orga-P concentrations measured in the outer estuary may  
537 also be related to the presence of bioturbation at this station (pers. obs.) - known to enhance  
538 organic matter degradation (Aller 1994) and to the higher degradability of marine compared to  
539 terrestrial organic matter. High  $\text{PO}_4^{3-}$  and low Fe-P concentrations may be due to the proximity of  
540 oceanic waters in the outer estuary. Indeed, the presence of sulfate-rich marine waters commonly  
541 leads to the formation of Fe sulfides in anoxic conditions, limiting Fe-P formation (Caraco et al.  
542 1989; Hyacinthe and Van Cappellen 2004). As expected, the increase in  $\text{NH}_4^+$  concentrations  
543 from the inner to the outer estuary in May, July and October may also be related to increasing  
544 salinity known to enhance  $\text{NH}_4^+$  desorption from particles (Hartzell et al. 2010).

545  $\text{NH}_4^+ : \text{PO}_4^{3-}$  ratios are expected to be close to the Redfield ratio (16) in conditions of  
546 organic matter regeneration. The  $\text{NH}_4^+ : \text{PO}_4^{3-}$  ratios < 16 (this study) provides evidence of Fe-P  
547 dissolution, as already shown in the Baltic Sea (Jilbert et al. 2011). This is confirmed by  
548 decreasing Fe-P and increasing  $\text{PO}_4^{3-}$  profiles. The general enhancement of pH and  $\text{OH}^-$   
549 concentrations from inner to outer estuaries ([http://www.donnees.bretagne.developpement-](http://www.donnees.bretagne.developpement-durable.gouv.fr)  
550 [durable.gouv.fr](http://www.donnees.bretagne.developpement-durable.gouv.fr)), the high pore water  $\text{Si}(\text{OH})_4$  concentrations (Fig. 5, A3) and the sulfate-enriched

551 marine waters are indeed expected to increase  $\text{PO}_4^{3-}$  desorption (Caraco et al. 1989; Mayer and  
552 Jarell 2000; Hyacinthe and Van Cappellen 2004). In spite of high pore water  $\text{PO}_4^{3-}$   
553 concentrations, Aut-P concentrations are generally lower ( $< 10 \mu\text{mol g}^{-1}$ ) in the outer than in the  
554 inner and mid estuary, in particular in February and May. The precipitation to Aut-P is rather  
555 limited by the low Orga-P and Fe-P concentrations (Fig. 4, A3) and the high  $\text{Mg}^{2+}$  concentrations  
556 of marine waters that compete with  $\text{Ca}^{2+}$  in outer brackish estuaries (Gunnars et al. 2004; Cao et  
557 al. 2007).

558

## 559 **5. Conclusion**

560

561 We highlight the influence of a combination of factors on benthic biogeochemical  
562 processes along a salinity gradient in a small macrotidal estuary. These results emphasize that P  
563 retention might be important in freshwater estuaries, due to favorable conditions to the  
564 precipitation of low reactive Aut-P (i.e. high organic and iron-bound P loads, anoxic conditions,  
565 low pH, sulfate and  $\text{Mg}^{2+}$  concentrations) and to the settlement of riverine P. In these freshwater  
566 conditions, we suggest that Aut-P precipitation could be additionally enhanced in Si-rich  
567 sediments by increasing the formation of Fe-P, a precursor of Aut-P. More studies are however  
568 needed to highlight that interactions between Si and P cycles could have a significant role in the  
569 long term storage of P. In the mid estuary, frequent erosion-deposition events, including  
570 translocation, lead to a succession of heterogeneous sediment layers and biogeochemical  
571 properties in point bar. More studies are needed to define seasonal origins of the deposited

572 matter, and erosion-deposition dynamics in point bars. Contrary to the inner and mid estuary, the  
573 outer estuary is representative of less perturbed and more marine ecosystems. This study  
574 emphasizes the strong estuarine gradient of benthic biogeochemical properties, and especially the  
575 long term storage of P in inner estuaries and high benthic stocks (and thus fluxes) of dissolved  
576 species, especially  $\text{NH}_4^+$  and  $\text{Si(OH)}_4$ , which have important implications for coastal ecosystems,  
577 and should be accounted for in ecological studies.

578 *Acknowledgements*

579

580           This work was supported by the French National Program for Coastal Environment  
581 (PNEC-EC2CO), the Conseil Général du Finistère and the Ministère de l'Enseignement Supérieur  
582 et de la Recherche. We gratefully thank the R/V Côtes de la Manche crew, Manon Le Goff,  
583 Agnès Youenou, Christophe Rabouille, Bruno Bombled and Julien Queré for their valuable aid  
584 for cores sampling and processing, Erwan Amice and Robert Marc for their helpfull assistance on  
585 board the *Hésione* (IUEM), Eric Legoff, Nicole Gouriou and Elisabeth Bruyant for their  
586 assistance at the hospital, Monique Briand for her help with figures, and Zosia Baumann for her  
587 language edition advices. We sincerely thank two reviewers and especially Tom Jilbert for his  
588 insightful critical comments and suggestions.

589 *References*

590

591 Allen GP, Salomon JC, Bassoullet P, Du Penhoat Y, de Grandpré C (1980) Effects of tides on  
592 mixing and suspended sediment transport in macrotidal estuaries. *Sediment. Geol.* 26(1-3):69-90

593 Aller RC (1994) Bioturbation and remineralization of sedimentary organic matter: effects of  
594 redox oscillation. *Chem. Geol.* 114(3-4):331-345

595 Aller RC (2004) Conceptual models of early diagenetic processes: The muddy seafloor as an  
596 unsteady, batch reactor. *J. Mar. Res.* 62:815-835

597 Aller RC, Mackin JE, Ullman WJ, Chen-Hou W, Shing-Min T, Jian-Cai J, Yong-Nian S, Jia-  
598 Zhen H (1985) Early chemical diagenesis, sediment-water solute exchange, and storage of  
599 reactive organic matter near the mouth of the Changjiang, East China Sea. *Cont. Shelf Res.*  
600 4(1/2):227-251

601 Aller RC, Heilbrun C, Panzeca C, Zhu Z, Baltzer F (2004) Coupling between sedimentary  
602 dynamics, early diagenetic processes, and biogeochemical cycling in the Amazon–Guianas  
603 mobile mud belt: coastal French Guiana. *Mar. Geol.* 208:331-360

604 Aminot A, Kérouel R, Coverly SC (2009). Nutrients in seawater using segmented flow analysis.  
605 In: Wurl O (ed.) *Practical guidelines for the analysis of seawater*. CRC Press, Boca Raton, USA,  
606 pp 143-178

607 Anderson FE, Black L, Watling LE, Mook W, Mayer LM (1981) A temporal and spatial study of  
608 mudflat erosion and deposition. *J. Sediment. Res.* 51:729-736

609 Andrieux F, Aminot A (1997) A two-year survey of phosphorus speciation in the sediments of  
610 the Bay of Seine (France). *Cont. Shelf Res.* 17:1229-1245

611 Andrieux-Loyer F, Philippon X, Bally G, K erouel R, Youenou A, Le Grand J (2008) Phosphorus  
612 dynamics and bioavailability in sediments of the Penz  Estuary (NW France): in relation to  
613 annual P-fluxes and occurrences of *Alexandrium Minutum*. Biogeochemistry 88(3):213-231  
614 Anschutz P, Zhong S, Sundby B, Mucci A, Gobeil C (1998) Burial efficiency of phosphorus and  
615 the geochemistry of iron in continental margin sediments. Limnol. Oceanogr. 43(1):53-64  
616 Aspila KI, Agemian H, Chau ASY (1976) A semi-automated method for the determination of  
617 inorganic, organic and total phosphate in sediments. The Analyst 101(1200):187-197  
618 Avil s A, Niell FX (2005) Pattern of phosphorus forms in a Mediterranean shallow estuary:  
619 Effects of flooding events. Estuar. Coast. Shelf Sci. 64(4):786-794  
620 Bassoulet P (1979) Etude de la dynamique des s diments en suspension dans l'estuaire de l'Aulne  
621 (rade de Brest). Ph.D. Thesis, Universit  de Bretagne Occidentale, Brest, France, 136 pp  
622 Berner RA (1980) Early diagenesis: a theoretical approach. Princeton University Press  
623 Berner RA, Rao JL (1993) Phosphorus in sediments of the Amazon River and estuary:  
624 Implications for the global flux of phosphorus to the sea. Geochim. Cosmochim. Acta  
625 58(10):2333-2339  
626 Beucher C, Treguer P, Corvaisier R, Hapette AM, Elskens M (2004) Production and dissolution  
627 of biosilica, and changing microphytoplankton dominance in the Bay of Brest (France). Mar.  
628 Ecol. Prog. Ser. 267:57-69  
629 Cao X, Harris WG, Josan MS, Nair VD (2007) Inhibition of calcium phosphate precipitation  
630 under environmentally-relevant conditions. Sci. Tot. Environ. 383:205-215  
631 Caraco NF, Cole JJ, Likens GE (1989) Evidence for sulfate-controlled phosphorus release from  
632 sediments of aquatic systems. Nature 341:316-318

633 Cloern JE (2001) Our evolving conceptual model of the coastal eutrophication problem. *Mar.*  
634 *Ecol. Prog. Ser.* 210:223-253

635 Conley DJ (2000) Biogeochemical nutrient cycles and nutrient management strategies.  
636 *Hydrobiol.* 410:87-96

637 Conley DJ, Schelske CL, Stoermer EF (1993) Modification of the biogeochemical cycle of silica  
638 with eutrophication. *Mar. Ecol. Prog. Ser.* 101:179-192

639 Day JW (1989) *Estuarine ecology.* Wiley-Interscience

640 De Montety L, Long B, Desrosiers G, Crémer J-F, Locat J, Stora G (2003) Utilisation de la  
641 scanographie pour l'étude des sédiments : influence des paramètres physiques, chimiques et  
642 biologiques sur la mesure des intensités tomographiques. *Can. J. Earth Sci.* 40:937-948

643 de Vicente I, Cruz-Pizarro L, Rueda, FJ (2010). Sediment resuspension in two adjacent shallow  
644 coastal lakes: controlling factors and consequences on phosphate dynamics. *Aquat. Sci.* 72(1):21-  
645 31

646 Dyer (1989) Estuarine flow interaction with topography - Lateral and longitudinal effects in  
647 Estuarine circulation. In: Neilson BJ, Kuo A, Brubaker J (ed) *Estuarine circulation.* Humana

648 Farmer VC, Delbos E, Miller JD (2005) The role of phytolith formation and dissolution in  
649 controlling concentrations of silica in soil solutions and streams. *Geoderma* 127(1-2):71-79

650 Findlay S, Howe K, Austin HK (1990) Comparison of Detritus Dynamics in Two Tidal  
651 Freshwater Wetlands. *Ecology* 71(1):288-295

652 Fontes MPF, Weed SB (1996) Phosphate adsorption by clays from Brazilian Oxisols:  
653 relationships with specific surface area and mineralogy. *Geoderma* 72:37-51

654 Froelich PN, Arthur MA, Burnett WC, Deakin M, Hensley V, Jahnke R, Kaul L, Kim KH, Roe

655 K, Soutar A, Vathakanon C (1988) Early diagenesis of organic matter in Peru continental margin  
656 sediments: Phosphorite precipitation. *Mar. Geol.* 80(3-4):309-343

657 Gagnoud M, Lajeunesse P, Desrosiers G, Long B, Dufour S, Labrie J, Mermillod-Blondin F,  
658 Stora G (2009) Litho- and biofacies analysis of postglacial marine mud using CT-scanning.  
659 *Engineering Geol.* 103:106-111

660 Gardner WS, McCarthy MJ (2009) Nitrogen dynamics at the sediment–water interface in  
661 shallow, sub-tropical Florida Bay: why denitrification efficiency may decrease with increased  
662 eutrophication. *Biogeochemistry* 95:185-198

663 Gehlen M, Van Raaphorst W (2002) The role of adsorption-desorption surface reactions in  
664 controlling interstitial Si(OH)<sub>4</sub> concentrations and enhancing Si(OH)<sub>4</sub> turn-over in shallow shelf  
665 seas. *Cont. Shelf Res.* 22(10):1529-1547

666 Gunnars A, Blomqvist S, Martinsson C (2004) Inorganic formation of apatite in brackish  
667 seawater from the Baltic Sea: an experimental approach. *Marine Chemistry* 91:15-26

668 Hartikainen H, Pitkänen M, Kairesalo T, Tuominen L (1996) Co-occurrence and potential  
669 chemical competition of phosphorus and silicon in lake sediment. *Wat. Res.* 30(10):2472-2477

670 Hartzell J, Jordan T, Cornwell J (2010) Phosphorus burial in sediments along the salinity gradient  
671 of the Patuxent River, a subestuary of the Chesapeake Bay (USA). *Estuar. Coasts* 33:92-106

672 Howarth RW, Marino R (2006) Nitrogen as the limiting nutrient for eutrophication in coastal  
673 marine ecosystems: evolving views over three decades. *Limnol. Oceanogr.* 51(1):364-376

674 Howarth R, Chan F, Conley DJ, Garnier J, Doney SC, Marino R, Billen G (2011) Coupled  
675 biogeochemical cycles: eutrophication and hypoxia in temperate estuaries and coastal marine  
676 ecosystems. *Front. Ecol. Environ.* 9(1):18-26

677 Hyacinthe C, Van Cappellen P (2004) An authigenic iron phosphate phase in estuarine  
678 sediments: composition, formation and chemical reactivity. *Mar. Chem.* 91(1-4):227-251

679 Jilbert T, Slomp CP, Gustafsson BG, Boer W (2011) Beyond the Fe-P-redox connection:  
680 preferential regeneration of phosphorus from organic matter as a key control on Baltic Sea  
681 nutrient cycles. *Biogeosciences* 8:1699-1720

682 Jordan TE, Cornwell JC, Boynton WR, Anderson JT (2008) Changes in phosphorus  
683 biogeochemistry along an estuarine salinity gradient: The iron conveyor belt. *Limnol. Oceanogr.*  
684 53(1):172-184

685 Khalil K, Raimonet K, Laverman AM, Yan C, Andrieux-Loyer F, Viollier E, Deflandre E,  
686 Ragueneau O, Rabouille C (submitted to *Aquatic Geochemistry*) Spatial and temporal variability  
687 of sediment organic matter recycling in two temperate small estuaries.

688 Koski-Vähälä J, Hartikainen H, Tallberg P (2001) Phosphorus Mobilization from Various  
689 Sediment Pools in Response to Increased pH and Silicate Concentration. *J. Environ. Quality*  
690 30:546-552

691 Laruelle GG (2009) Quantifying nutrient cycling and retention in coastal waters at the global  
692 scale. Ph.D. Thesis, Utrecht University, Utrecht, Netherlands, 226 pp

693 Laverman A, Van Cappellen P, van Rotterdam-Los D, Pallud C, Abell J (2006) Potential rates  
694 and pathways of microbial nitrate reduction in coastal sediments. *FEMS Microbiol. Ecol.* 58:179-  
695 192

696 Lehtoranta J, Heiskanen A-S (2003) Dissolved iron:phosphate ratio as an indicator of phosphate  
697 release to oxic water of the inner and outer coastal Baltic Sea. *Hydrobiologia* 492(1-3):69-84

698 Lesourd S, Lesueur P, Brun-Cottan JC, Garnaud S, Poupinet N (2003) Seasonal variations in the

699 characteristics of superficial sediments in a macrotidal estuary (the Seine inlet, France). *Estuar.*  
700 *Coast. Shelf Sci.* 58(1):3-16

701 Lijklema L (1977) The role of iron in the exchange of phosphorus between water and sediments.  
702 In: Golterman HL (ed.) *Interactions between sediments and fresh water. Proc. Int. Symp.,*  
703 *Amsterdam, the Netherlands. 6–10 Sept. The Hague, the Netherlands, pp 313-317*

704 Loucaides S, Michalopoulos P, Presti M, Koning E, Behrends T, Van Cappellen P (2010)  
705 *Seawater-mediated interactions between diatomaceous silica and terrigenous sediments: Results*  
706 *from long-term incubation experiments. Chem. Geol.* 270:68-79

707 Louchouart P, Lucotte M, Duchemin E, de Vernal A (1997) Early diagenetic processes in recent  
708 sediments of the Gulf of St-Lawrence: phosphorus, carbon and iron burial rates. *Mar. Geol.*  
709 139:181-200

710 Matijević S, Bojanić N, Kušpilić G, Ninčević Gladan Z (2009) Seasonal variations of phosphorus  
711 species in sediment from the middle Adriatic Sea. *Environ. Earth Sci.* 59:853-866

712 Mayer LM, Gloss SP (1980) Buffering of silica and phosphate in a turbid river. *Limnol.*  
713 *Oceanogr.* 25(1):12-22

714 Mayer TD, Jarrell WM (2000) Phosphorus sorption during iron(II) oxidation in the presence of  
715 dissolved silica. *Wat. Res.* 34(16):3949-3956

716 Michalopoulos P, Aller RC (2004) Early diagenesis of biogenic silica in the Amazon delta:  
717 alteration, authigenic clay formation, and storage. *Geochim. Cosmochim. Acta* 68(5):1061-1085

718 Michaud E, Desrosiers G, Long B, de Montety L, Crémer J-F, Pelletier E, Locat J, Gilbert F,  
719 Stora G (2003) Use of axial tomography to follow temporal changes of benthic communities in  
720 an unstable sedimentary environment (Ha!Ha! Bay, Saguenay Fjord). *J. Exp. Mar. Biol. Ecol.*

721 285/286:265-282

722 Moreno S, Niell FX (2004) Scales of variability in the sediment chlorophyll content of the  
723 shallow Palmones River Estuary, Spain. *Estuar. Coast. Shelf Sci.* 60(1):49-57

724 Nelson DM, Treguer P, Brzezinski MA, Leynaert A, Queguiner B (1995) Production and  
725 dissolution of biogenic silica in the ocean: Revised global estimates, comparison with regional  
726 data and relationship to biogenic sedimentation. *Global Biogeochem. Cycles* 9(3):359-372

727 Némery J, Garnier J (2006) Typical features of particulate phosphorus in the Seine estuary  
728 (France). *Hydrobiologia* 588:271-290

729 Postma (1967) Sediment transport and sedimentation in the estuarine environment. In: *Estuaries,*  
730 *American association for the advancement of science. Washington, pp 158-179*

731 Prastka K, Sanders R, Jickells T (1998) Has the role of estuaries as sources or sinks of dissolved  
732 inorganic phosphorus changed over time? Results of a  $K_d$  study. *Mar. Poll. Bull.* 36(9):718-728

733 Querné J (2011) Invasion de *Spartina alterniflora* dans les marais de la rade de Brest.  
734 Comportement invasif et impact sur le cycle biogéochimique du silicium. Ph.D thesis, Université  
735 de Bretagne Occidentale, Brest, France, 217 pp

736 Ragueneau O, Lancelot C, Egorov V, Vervlimmeren J, Cociasu A, Déliat G, Krastev A, Daoud  
737 N, Rousseau V, Popovitchev V, Brion N, Popa L, Cauwet G (2002) Biogeochemical  
738 Transformations of Inorganic Nutrients in the Mixing Zone between the Danube River and the  
739 North-western Black Sea. *Estuar. Coast. Shelf Sci.* 54(3):321-336

740 Raimonet (2011) Cycle benthique du silicium dans les estuaires : observations et modélisation à  
741 différentes échelles spatio-temporelles. Ph.D. Thesis, Université de Bretagne Occidentale, Brest,  
742 France, 167 pp

743 Raimonet M, Ragueneau O, Andrieux-Loyer F, Philippon X, Kerouel R, Le Goff M, Mémery L  
744 (2013) Spatio-temporal variability in benthic silica cycling in two macrotidal estuaries: causes  
745 and consequences for local to global studies. *Estuar. Coast. Shelf Sci.* 119:31-43

746 Rao JL, Berner RA (1997) Time variations of phosphorus and sources of sediments beneath the  
747 Chang Jiang (Yangtze River). *Mar. Geol.* 139:95-108

748 Reimers CE, Ruttenberg KC, Canfield DE, Christiansen MB, Martin JB (1996) Porewater pH and  
749 authigenic phases formed in the uppermost sediments of the Santa Barbara Basin. *Geochim.*  
750 *Cosmochim. Acta* 60(21):4037-4057

751 Resing JA, Mottl MJ (1992) Determination of manganese in seawater using flow injection  
752 analysis with on-line preconcentration and spectrophotometric detection. *Anal. Chem.*  
753 64(22):2682-2687

754 Ruttenberg KC (1992) Development of a sequential extraction method for different forms of  
755 phosphorus in marine sediments. *Limnol. Oceanog.* 37(7):1460-1482

756 Ruttenberg KC, Berner RA (1993) Authigenic apatite formation and burial in sediments from  
757 non-upwelling, continental margin environments. *Geochim. Cosmochim. Acta* 57(5):991-1007

758 Sarradin P-M, Le Bris N, Le Gall C, Rodier P (2005) Fe analysis by the ferrozine method:  
759 Adaptation to FIA towards in situ analysis in hydrothermal environment. *Talanta* 66(5):1131-  
760 1138

761 Seitzinger SP, Harrison JA, Dumont E, Beusen AHW, Bouwman AF (2005) Sources and delivery  
762 of carbon, nitrogen, and phosphorus to the coastal zone: An overview of Global Nutrient Export  
763 from Watersheds (NEWS) models and their application. *Global Biogeochem. Cycles*  
764 19(4):GB4S01-GB04S01

765 Sharp JH, Pennock JR, Church TM, Tramontano JM, Cifuentes LA (1984). The estuarine  
766 interaction of nutrients, organics, and metals: A case study in the Delaware Estuary.  
767 In: Kennedy VS (ed) The estuary as a filter. Academic Press, Orlando, pp 241-258  
768 Slomp K, Epping E, Helder W, Van Raaphorst W (1996) A key role for iron-bound phosphorus  
769 in authigenic apatite formation in North Atlantic continental platform sediments. *J. Mar. Res.*  
770 54(6):1179-1205  
771 Smetacek VS (1985) Role of sinking in diatom life-history cycles: ecological, evolutionary and  
772 geological significance. *Mar. Biol.* 84(3):239-251  
773 Smith SV (1984) Phosphorus versus nitrogen limitation in the marine environment. *Limnol.*  
774 *Oceanog.* 29:1149-1160  
775 Soetaert K, Herman PMJ, Middelburg JJ, Heip C (1998) Assessing organic matter mineralization,  
776 degradability and mixing. *J. Mar. Res.* 56(2):519-534  
777 Soetaert K, Middelburg JJ, Herman PMJ, Buis K (2000) On the coupling of benthic and pelagic  
778 biogeochemical models. *Earth-Sci. Rev.* 51(1-4):173-201  
779 Sundareshwar PV, Morris JT (1999) Phosphorus sorption characteristics of intertidal marsh  
780 sediments along an estuarine salinity gradient. *Limnol. Oceanog.* 44(7):1693-1701  
781 Sundby B, Gobeil C, Silverberg N, Mucci A (1992) The phosphorus cycle in coastal marine  
782 sediments. *Limnol. Oceanog.* 37(6):1129-1145  
783 Tallberg P, Tréguer P, Beucher C, Corvaisier R (2008) Potentially mobile pools of phosphorus  
784 and silicon in sediment from the Bay of Brest: Interactions and implications for phosphorus  
785 dynamics. *Estuar. Coast. Shelf Sci.* 76(1):85-94  
786 Thibodeau B, Lehmann MF, Kowarzyk J, Mucci A, d, Gélinas Y, Gilbert D, Maranger R,

787 Alkhatib M (2010) Benthic nutrient fluxes along the Laurentian Channel: Impacts on the N  
788 budget of the St. Lawrence marine system. *Estuar. Coast. Shelf Sci.* 90:195-205

789 Tréguer P, Le Corre, P (1975) Manuel d'analyse des sels nutritifs dans l'eau de mer: utilisation  
790 de l'auto-analyseur Technicon II. Université de Bretagne Occidentale, Brest, France

791 Tuominen L, Hartikainen H, Kairesalo T, Tallberg P (1997) Increased bioavailability of sediment  
792 phosphorus due to silicate enrichment. *Wat. Res.* 32(7):2001-2008

793 Tyson RV, Pearson TH (1991) Modern and ancient continental shelf anoxia: an overview.  
794 Geological Society, London, Special Publications 58:1-24

795 Violante A, Pigna M, Ricciardella, Gianfreda (2002) Adsorption of phosphate on variable charge  
796 minerals and soils as affected by organic and inorganic ligands. *Dev. Soil Sci.* 28(1):279-295

797 Woodruff JD, Geyer WR, Sommerfield CK, Driscoll NW (2001) Seasonal variation of sediment  
798 deposition in the Hudson River estuary. *Mar. Geol.* 179(1-2):105-119

799 Yamada SS, D'Elia CF (1984) Silicic acid regeneration from estuarine sediment cores. *Mar. Ecol.*  
800 *Prog. Ser.* 18(1-2):113-118

801 *Tables*

802

803 Table 1: Environmental parameters in the inner (A1), mid (A2) and outer (A3) Aulne Estuary in  
 804 February, May, July and October 2009. General parameters are the Aulne River discharge Q, the  
 805 tidal range in Brest, and the water depth D at each station. Overlying waters are characterized by  
 806 temperature T, salinity S, total suspended sediment TSS, and concentrations of (NO<sub>3</sub><sup>-</sup>+NO<sub>2</sub><sup>-</sup>),  
 807 NH<sub>4</sub><sup>+</sup>, PO<sub>4</sub><sup>3-</sup> and Si(OH)<sub>4</sub> (n=3). The grain size (% < 63 μm) of surface sediment is also given  
 808 (n=3).

Station	Sampling date	Q (m <sup>3</sup> s <sup>-1</sup> )	Tidal range (m)	D (m)	T (°C)	S (-)	TSS (mg l <sup>-1</sup> )	(NO <sub>3</sub> <sup>-</sup> +NO <sub>2</sub> <sup>-</sup> )	NH <sub>4</sub> <sup>+</sup>	PO <sub>4</sub> <sup>3-</sup>	Fe <sup>2+</sup>	Mn <sup>2+</sup>	Si(OH) <sub>4</sub>	< 63 μm (%)
											(μM)			
A1	14/02/2009	64.6	5.2	2.5	7.7	0		546	3	0.3	1.3	0.2	97	78 ± 6
	07/05/2009	10.4	5.1	2	14.4	0	45	333	4	0.6	3.8	0.4	120	82 ± 2
	25/07/2009	4.24	6.2	0.5	19.7	0	248	242	4	0.9	1.0	0.4	98	82 ± 3
	30/10/2009	3.67	3.7	1	14.2	8.7	182	384	5	2.3	1.9	0.4	111	82 ± 3
A2	15/02/2009	54.1	4.2	3	7.4	13.7		392	2	0.6	0.2	0.3	79	51 ± 6
	08/05/2009	9.95	5.2	3	14	22.5	39	122	3	0.7	0.2	0.4	44	64 ± 8
	24/07/2009	5.01	6.4	1.5	19.5	27.5	33	47	5	1.1	0.3	1.0	17	42 ± 8
	31/10/2009	3.47	4.5	1	15.5	29.9	33	46	11	1.7	0.3	0.2	29	37 ± 4
A3	16/02/2009	49.7	3.2	1.75	8	20		199	2	0.6	0.1	0.2	53	74 ± 3
	06/05/2009	10.7	4.7	2	13.5	24.6	21	86	3	0.4	0.2	0.3	31	74 ± 3
	26/07/2009	3.59	5.7	3	19.1	30.9	48	25	4	1.0	0.3	0.4	12	71 ± 8
	01/11/2009	4.91	5	2.5	15	33	20	7	4	0.8	0.3	0.1	16	73 ± 1

809

810

811 Table 2: Statistical t-test for seasonal changes of grain size ( $\% < 63 \mu\text{m}$ ) and porosity ( $\phi$ ) in

812 surface sediments in the inner Aulne Estuary (station A1,  $n=3$ ).

	$\% < 63 \mu\text{m}$		$\phi$	
	Shapiro test $p=0.03$		Shapiro test $p=0.023$	
	$t$	$p$	$t$	$p$
Feb ~ May	-1.14	0.357	-5.91	0.01
Feb ~ Jul	-1.055	0.367	-6.13	0.021
Feb ~ Oct	-1.176	0.33	-4.72	0.042

813

814

815 Table 3: Correlations between surface sediment properties along the Aulne Estuary (stations A1,

816 A2 and A3). n=12 (P forms) or 36 (dissolved forms). Significant correlations ( $p<0.5$ ) are in **bold**.

		(NO <sub>3</sub> <sup>-</sup> +NO <sub>2</sub> <sup>-</sup> )	NH <sub>4</sub> <sup>+</sup>	PO <sub>4</sub> <sup>3-</sup>	Fe <sup>2+</sup>	Mn <sup>2+</sup>	Si(OH) <sub>4</sub>	φ	Fe-P	Aut-P	Det-P
Station A1	NH <sub>4</sub> <sup>+</sup>	-0.216									
	PO <sub>4</sub> <sup>3-</sup>	0.15	<b>-0.605</b>								
	Fe <sup>2+</sup>	-0.242	<b>0.741</b>	<b>-0.578</b>							
	Mn <sup>2+</sup>	<b>-0.442</b>	<b>0.75</b>	<b>-0.726</b>	<b>0.79</b>						
	Si(OH) <sub>4</sub>	<b>-0.4</b>	<b>0.787</b>	<b>-0.503</b>	<b>0.892</b>	<b>0.82</b>					
	φ	0.032	<b>-0.602</b>	0.176	<b>-0.513</b>	<b>-0.473</b>	<b>-0.644</b>				
	Fe-P	<b>0.477</b>	<b>-0.525</b>	0.27	<b>-0.656</b>	<b>-0.558</b>	<b>-0.738</b>	<b>0.415</b>			
	Aut-P	-0.088	<b>0.711</b>	<b>-0.736</b>	<b>0.695</b>	<b>0.575</b>	<b>0.674</b>	<b>-0.395</b>	<b>-0.48</b>		
	Det-P	-0.273	0.227	<b>-0.592</b>	<b>0.363</b>	<b>0.594</b>	0.266	<b>-0.362</b>	<b>-0.389</b>	<b>0.378</b>	
	Orga-P	<b>0.479</b>	<b>-0.342</b>	0.251	<b>-0.396</b>	<b>-0.477</b>	<b>-0.481</b>	<b>0.641</b>	<b>0.506</b>	<b>-0.335</b>	<b>-0.433</b>
Station A2	NH <sub>4</sub> <sup>+</sup>	-0.278									
	PO <sub>4</sub> <sup>3-</sup>	-0.193	<b>0.452</b>								
	Fe <sup>2+</sup>	-0.078	-0.025	-0.07							
	Mn <sup>2+</sup>	-0.207	0.073	-0.095	<b>0.83</b>						
	Si(OH) <sub>4</sub>	-0.24	<b>0.381</b>	<b>0.398</b>	<b>0.791</b>	<b>0.7</b>					
	φ	0.347	<b>-0.63</b>	-0.327	0.091	-0.083	-0.136				
	Fe-P	0.135	<b>-0.582</b>	<b>-0.441</b>	-0.227	<b>-0.386</b>	<b>-0.471</b>	<b>0.369</b>			
	Aut-P	-0.265	0.014	-0.112	0.056	-0.118	0.109	-0.234	<b>0.555</b>		
	Det-P	-0.251	0.049	-0.233	0.093	0.162	0.013	<b>-0.456</b>	0.253	<b>0.336</b>	
	Orga-P	0.127	-0.179	0.048	0.092	0.112	-0.052	<b>0.449</b>	-0.102	<b>-0.518</b>	-0.155
Station A3	NH <sub>4</sub> <sup>+</sup>	-0.237									
	PO <sub>4</sub> <sup>3-</sup>	-0.192	<b>0.929</b>								
	Fe <sup>2+</sup>	-0.247	<b>-0.497</b>	<b>-0.436</b>							
	Mn <sup>2+</sup>	<b>-0.494</b>	-0.041	-0.045	0.15						
	Si(OH) <sub>4</sub>	-0.39	<b>0.934</b>	<b>0.835</b>	-0.259	-0.044					
	φ	<b>0.499</b>	<b>-0.408</b>	-0.273	-0.107	-0.083	<b>-0.597</b>				
	Fe-P	<b>0.305</b>	<b>-0.576</b>	-0.471	0.159	0.236	<b>-0.678</b>	<b>0.646</b>			
	Aut-P	0.144	0.281	0.204	<b>-0.349</b>	-0.109	0.194	0.213	0.098		
	Det-P	-0.269	<b>0.351</b>	0.257	-0.266	0.353	<b>0.291</b>	0.024	-0.155	<b>0.307</b>	
	Orga-P	<b>0.458</b>	<b>-0.367</b>	<b>-0.297</b>	-0.1	<b>-0.45</b>	<b>-0.508</b>	<b>0.459</b>	<b>0.345</b>	0.054	<b>-0.461</b>

817

818

819 Table 4: Summary of Auth-P, Fe-P, Orga-P, Det-P concentrations ( $\mu\text{mol g}^{-1}$ ) and  $\text{Si(OH)}_4$ 820 concentrations ( $\mu\text{M}$ ) in freshwater, estuarine and marine ecosystems. All P forms were extracted

821 with the SEDEX method (modified or not).

Site	System type	Auth-P	Orga-P	Fe-P	Det-P	$\text{Si(OH)}_4$	Reference
		$(\mu\text{mol g}^{-1})$				$(\mu\text{M})$	
Middle Adriatic	marine	0-2.7	1.5-5.4	1.9-11.9	0.4-3.4		Matijević et al. (2009)
Patuxent River Estuary	brackish	1-4.5	4-10	15-55	2-4.5		Jordan et al. (2008)
St Laurent Gulf	marine	8.6-13.6	4-5	7-28		200*	Louchouart et al. (1997) *Thibodeau et al. (2010)
Amazon River	fresh mixing zone	4.7 3.6	4.5 4.3	4.1 7.5	2.2 1.0	50-250*	Berner and Rao (1993) *Michalopoulos and Aller (2004)
Penzé Estuary	inner estuary outer estuary	8-12 1.5-2	17 2	22 2	up to 8.6 4-5		Andrieux-Loyer et al. (2008)
Yangtze River	fresh	1.7-8.2	0.6-2.8	0.1-3.7	1.1-12.6	200-600*	Rao and Berner (1997) *Aller et al. (1985)

822

# Figures

Figure 1: Location of stations A1, A2 and A3 along the Aulne Estuary.

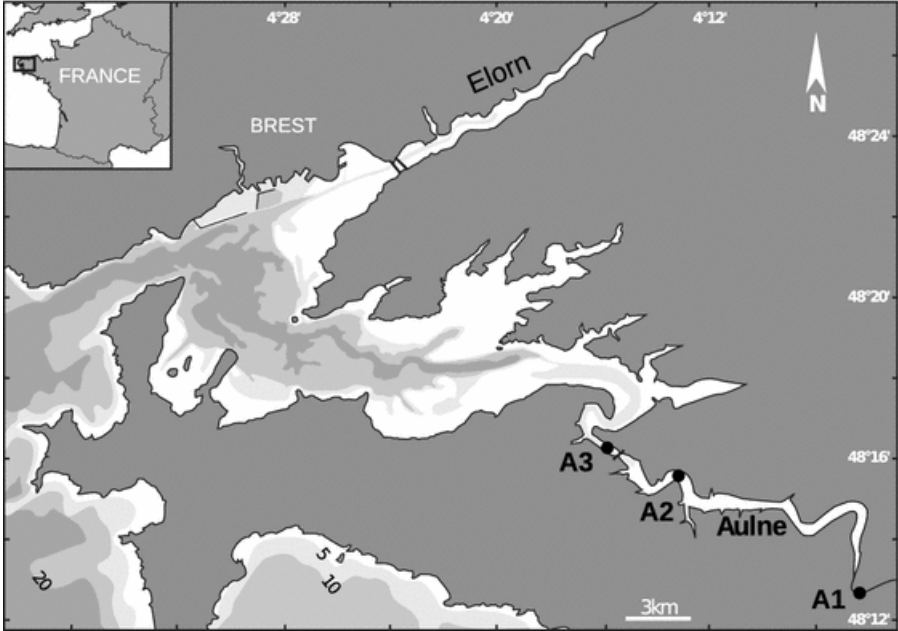


Figure 2: Aulne River discharge ( $m^3 s^{-1}$ ) at Chateaulin in 2009. Source: DREAL Bretagne/HYDROMEDD/DE. Sampling periods are represented by grey areas.

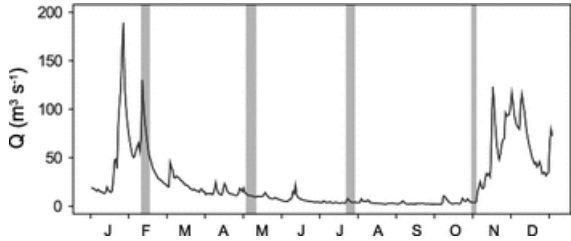


Figure 3: Vertical profiles of porosity and tomographic intensity (TI, HU) and bi-dimensional CT scan pictures from the inner to the outer Aulne Estuary (stations A1, A2 and A3, rows) in February, May, July and October 2009 (columns). Horizontal dashed lines illustrate the temporal evolution of specific layers described in the text. Fluid muds and sediment deposition are indicated on CT scan pictures.

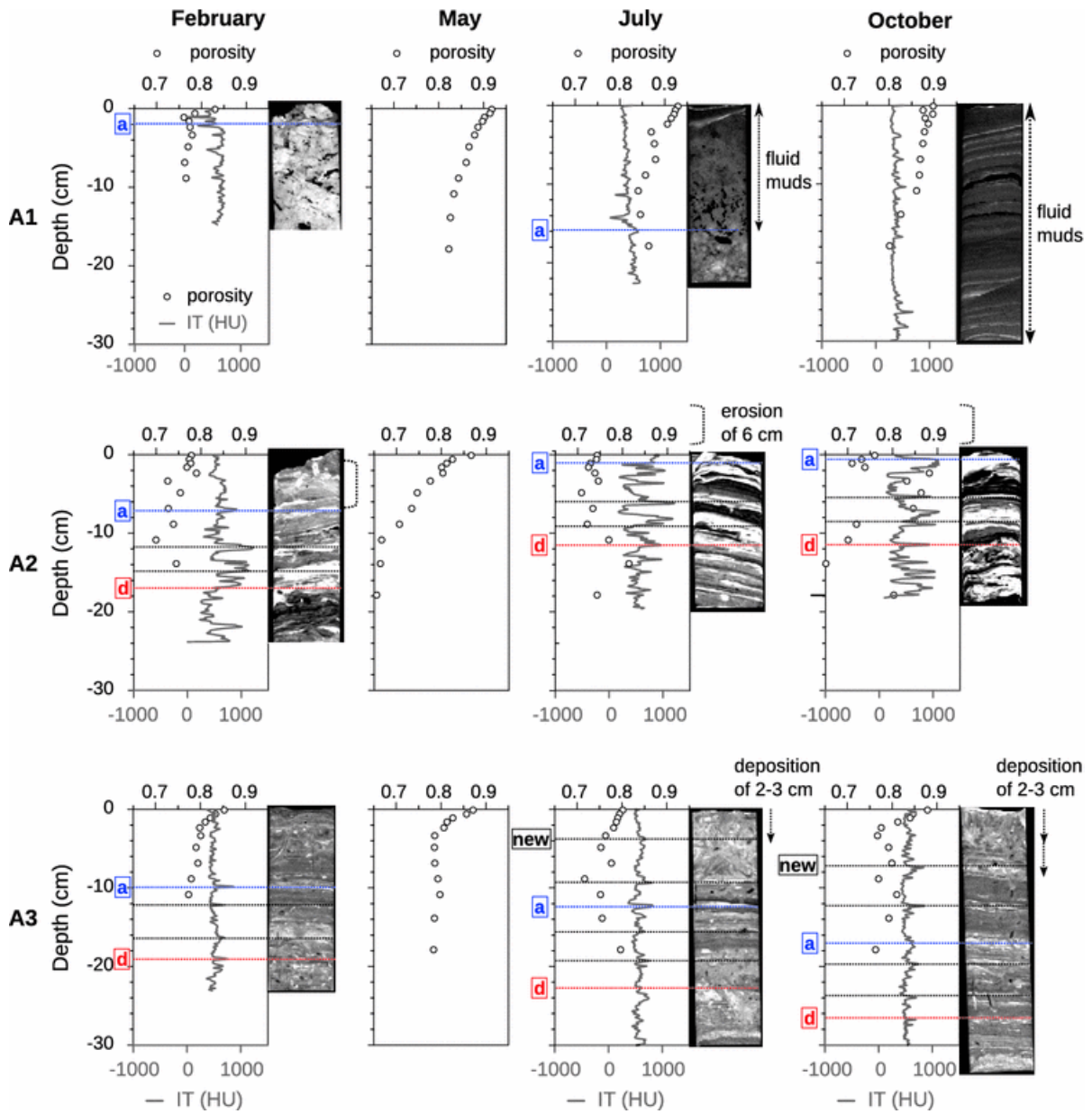


Figure 4: Contour maps of phosphorus forms (rows: Orga-P, Fe-P, Aut-P, Det-P;  $\mu\text{mol g}^{-1}$ ) in benthic sediments along the Aulne Estuary (columns: A1, A2 and A3) in 2009. Measured values are represented by black points ( $n=1$ ) in February, May, July and October. The horizontal dashed lines represent the temporal evolution of specific layers observed in Fig. 3.

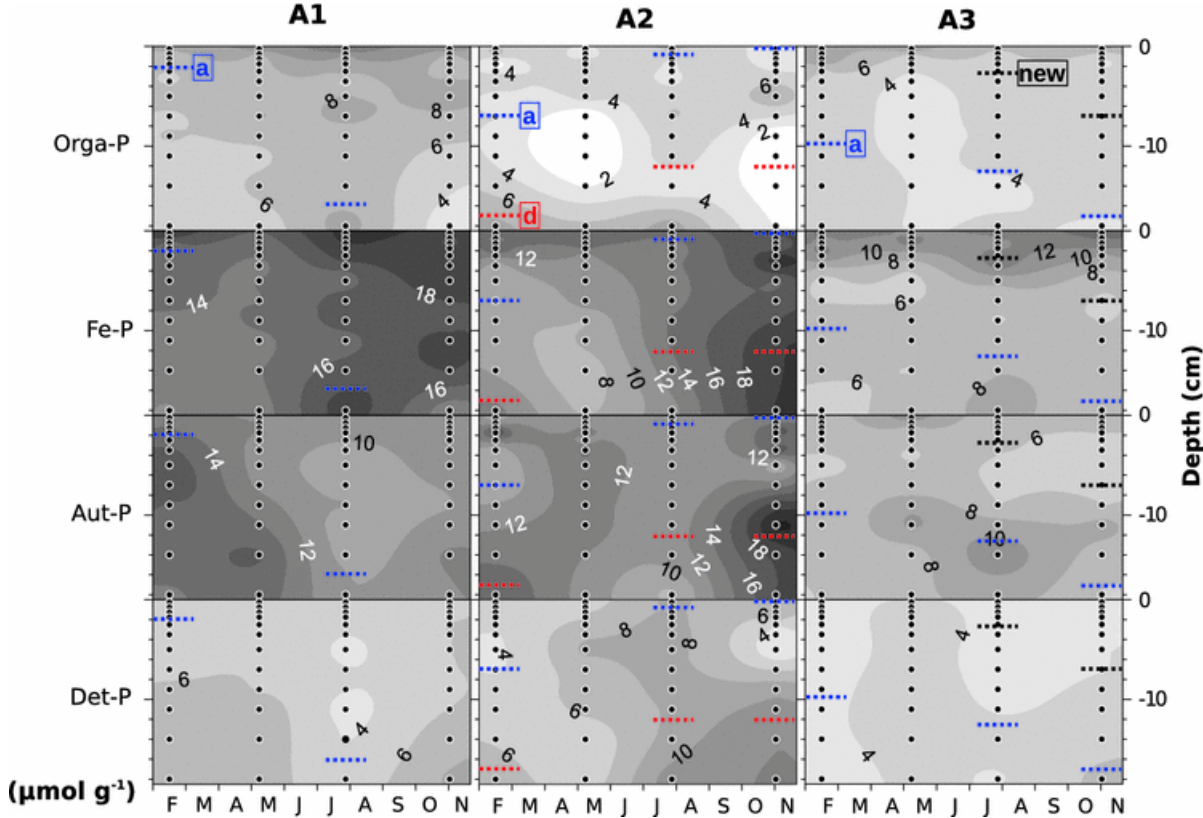


Figure 5: Contour maps of dissolved species concentrations (rows:  $\text{PO}_4^{3-}$ ,  $\text{NH}_4^+$ ,  $\text{Si(OH)}_4$ ,  $\text{NO}_3^-$ ,  $\text{NO}_2^-$ ,  $\text{Fe}^{2+}$ ,  $\text{Mn}^{2+}$ ;  $\mu\text{M}$ ) in pore waters along the Aulne Estuary (columns: A1, A2 and A3) in 2009. Measured values are represented by black points (n=3) in February, May, July and October.

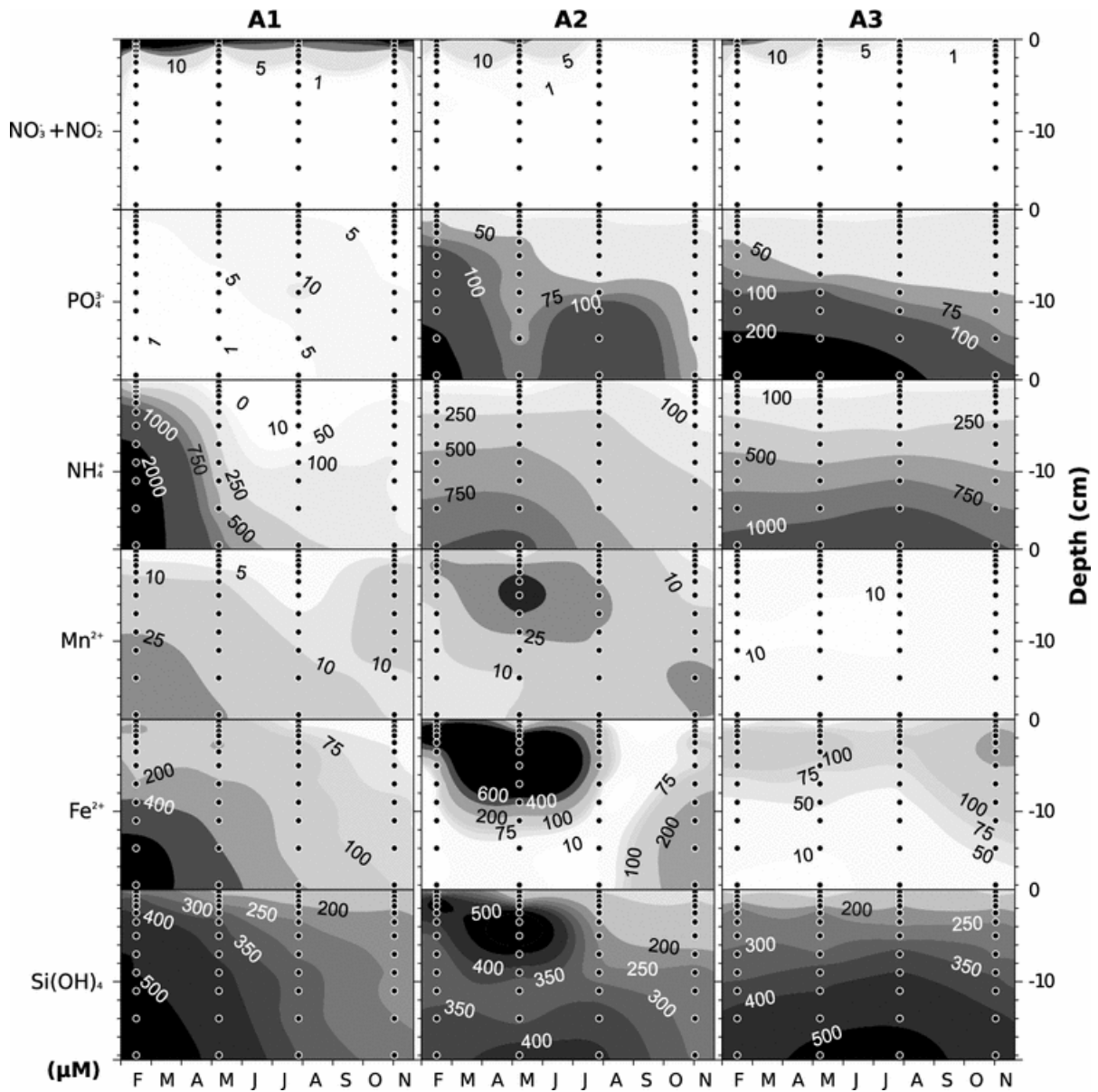


Figure 6: Contour maps of dissolved species molar ratios (rows:  $\text{NH}_4^+:\text{PO}_4^{3-}$ ,  $\text{Fe}^{2+}:\text{PO}_4^{3-}$ ) in pore waters along the Aulne Estuary (columns: A1, A2 and A3) in 2009 (rows). Measured values are represented by black points ( $n=3$ ) in February, May, July and October.

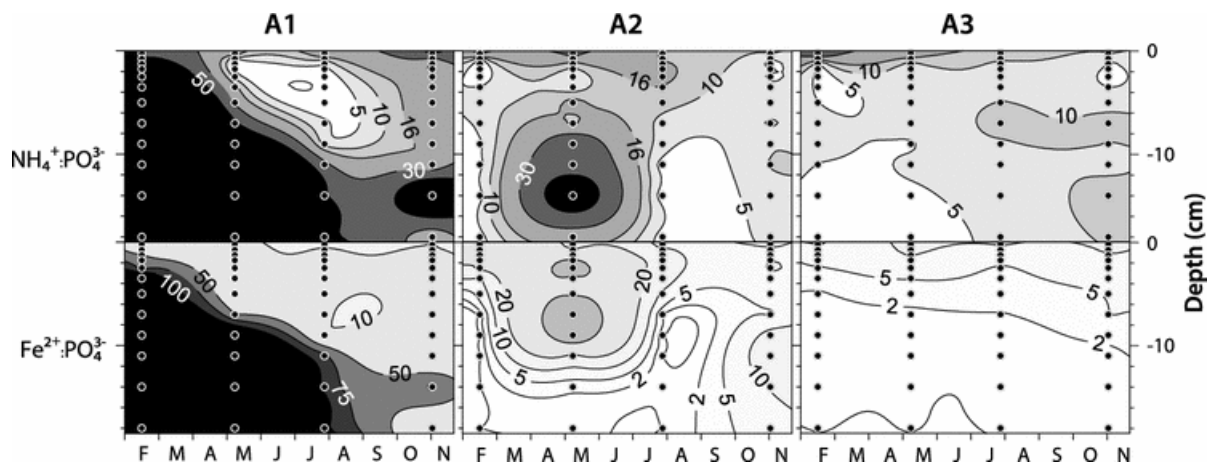


Figure 7: Vertical profiles of  $\text{NH}_4^+:\text{PO}_4^{3-}$  and  $\text{Fe}^{2+}:\text{PO}_4^{3-}$  ratios,  $\text{PO}_4^{3-}$  and  $\text{Si}(\text{OH})_4$  concentrations ( $\mu\text{M}$ ), Orga-P, Fe-P and Aut-P concentrations ( $\mu\text{mol g}^{-1}$ ) at station A1 in February and at station A2 in October.

